ON THE VLASOV-MAXWELL SYSTEM WITH A STRONG EXTERNAL MAGNETIC FIELD

Francis Filbet, Tao Xiong, Eric Sonnendr¨uckersonnendr¨ Sonnendr¨ucker

▶ **To cite this version:**

Francis Filbet, Tao Xiong, Eric Sonnendr¨uckersonnendr¨ Sonnendr¨ucker. ON THE VLASOV-MAXWELL SYSTEM WITH A STRONG EXTERNAL MAGNETIC FIELD. SIAM Journal on Applied Mathematics, 2018, 78 (2), pp.1030-1055. hal-01437310

HAL Id: hal-01437310
https://hal.science/hal-01437310

Submitted on 17 Jan 2017

HAL is a multi-disciplinary open access archive for the deposit and dissemination of scientific research documents, whether they are published or not. The documents may come from teaching and research institutions in France or abroad, or from public or private research centers.

L'archive ouverte pluridisciplinaire **HAL**, est destinée au dépôt et à la diffusion de documents scientifiques de niveau recherche, publiés ou non, émanant des établissements d'enseignement et de recherche français ou étrangers, des laboratoires publics ou privés.

Distributed under a Creative Commons Attribution - NonCommercial 4.0 International License

ON THE VLASOV-MAXWELL SYSTEM WITH A STRONG EXTERNAL MAGNETIC FIELD

FRANCIS FILBET, TAO XIONG AND ERIC SONNENDRÜCKER

Abstract. This paper establishes the long time asymptotic limit of the $2d \times 3d$ Vlasov-Maxwell system with a strong external magnetic field. Hence, a guiding center approximation is obtained in the two dimensional case with a self-consistent electromagnetic field given by Poisson type equations. Then, we propose a high order approximation of the asymptotic model and perform several numerical experiments which provide a solid validation of the method and illustrate the effect of the self-consistent magnetic field on the current density.

Keywords. Asymptotic limit; High order scheme; Vlasov-Maxwell system; Finite difference methods.

Contents

1. Introduction 1
2. Mathematical modeling 3
2.1. Rescaling of the Vlasov-Maxwell system 3
2.2. Asymptotic limit of the Vlasov-Maxwell system 5
2.3. Weak solutions for the asymptotic model 10
2.4. Guiding center model & linear instability 13
3. Numerical scheme 14
3.1. Hermite WENO finite difference scheme for the transport equation 14
3.2. Discretization of the elliptic equations 16
4. Numerical Examples 16
4.1. Linear equation 16
4.2. Diocotron instability 17
4.3. Kelvin-Helmholtz instability 20
5. Conclusion 23
Acknowledgement 24
References 25

1. Introduction

We consider a plasma confined by a strong external magnetic field, hence the charged gas evolves under its self-consistent electromagnetic field and the confining magnetic field. This configuration is typical of a tokamak plasma [3, 30], where the magnetic field is used to confine particles inside the core of the device.

We assume that on the time scale we consider, collisions can be neglected both for ions and electrons, hence collective effects are dominant and the plasma is entirely modelled with kinetic transport equations, where the unknown is the number density of particles $f \equiv f(t, \mathbf{x}, \mathbf{v})$ depending on time $t \geq 0$, position $\mathbf{x} \in D \subset \mathbb{R}^3$ and velocity $\mathbf{v} \in \mathbb{R}^3$.

Such a kinetic model provides an appropriate description of turbulent transport in a fairly general context, but it requires to solve a six dimensional problem which leads to a huge computational cost. To reduce the cost of numerical simulations, it is classical to derive asymptotic models with a smaller number of variables than the kinetic description. Large magnetic fields usually lead to the so-called drift-kinetic limit [1, 8, 28, 27] and we refer to [4, 7, 19, 20, 14, 21] for recent mathematical results

on this topic. In this regime, due to the large applied magnetic field, particles are confined along the magnetic field lines and their period of rotation around these lines (called the cyclotron period) becomes small. It corresponds to the finite Larmor radius scaling for the Vlasov-Poisson equation, which was introduced by Frénod and Sonnendrücker in the mathematical literature [19, 20]. The two-dimensional version of the system (obtained when one restricts to the perpendicular dynamics) and the large magnetic field limit were studied in [14] and more recently in [4, 31, 24]. We also refer to the recent work [26] of Hauray and Nouri, dealing with the well-posedness theory with a diffusive version of a related two dimensional system. A version of the full three dimensional system describing ions with massless electrons was studied by Han-Kwan in [23, 25].

Here we formally derive a new asymptotic model under both assumptions of large magnetic field and large time asymptotic limit for the two dimensional in space and three dimensional in velocity ($2d \times 3d$) Vlasov-Maxwell system. An analogous problem for the Vlasov-Poisson system has already been carefully studied by F. Golse and L. Saint-Raymond in two dimension [21, 32, 22], and recently by P. Degond and F. Filbet in three dimension [12]. In this paper, we will follow [12] to introduce some main characteristic scales to rewrite the Vlasov-Maxwell system in a dimensionless form, and reformulate the Maxwell equations by defining two potential functions corresponding to the self-consistent electromagnetic field. We consider a small cyclotron period, where the plasma frequency is relatively small as compared to the cyclotron frequency, and study the long time behavior of the plasma. Assuming a constant strong external magnetic field and that the distribution function is homogeneous along the external magnetic field, an asymptotic kinetic model can be derived by performing Hilbert expansions and comparing the first three leading order terms in terms of the small cyclotron period, thanks to passing in the cylindrical coordinates. The new asymptotic model is composed of two two dimensional transport equations for the distribution functions of ions and electrons respectively, averaging in the velocity plane orthogonal to the external magnetic field, and a Poisson's equation for determining the electric potential as well as an elliptic equation for the magnetic potential. It is incompressible with a divergence free transport velocity and shares several good features with the original Vlasov-Maxwell system, such as conservation of moments in velocity, total energy, as well as the L^p norm and physical bounds. The existence of weak solutions for the asymptotic model can also be obtained by following the lines of existence of weak solutions for the Vlasov-Poisson system [2, 13], with some L^p estimates on the charge density and current. Moreover, as the Mach number goes to 0 in the self-consistent magnetic field, we can recover the two dimensional guiding-center model, which is an asymptotic model for the Vlasov-Poisson system under the same scalings [21, 36, 29].

A high order numerical scheme will be proposed for solving the new asymptotic model, which is an extension of the one developed by C. Yang and F. Filbet [36] for the two dimensional guiding center model. Some other recent numerical methods for the Vlasov-Poisson system or the two dimensional guiding-center model can be referred to [15, 34, 10, 9, 18, 16, 35] and reference therein. Here a Hermite weighted essentially non-oscillatory (HWENO) scheme is adopted for the two dimensional transport equation, as well as the fast Fourier transform (FFT) or a 5-point central difference scheme for the Poisson equation of the electric potential and the 5-point central difference scheme for the elliptic equation of the magnetic potential. We will compare the asymptotic kinetic model with the two dimensional guiding-center model. With some special initial datum as designed in the numerical examples, we will show that under these settings, the two dimensional guiding-center model stays steady or nearly steady, while the asymptotic model can create some instabilities with a small initial nonzero current for the self-magnetic field. These instabilities are similar to some classical instabilities, such as Kelvin-Helmholtz instability [18], diocotron instability [36] for the two dimensional guiding-center model with some other perturbed initial conditions, which can validate some good properties of our new asymptotic model.

The rest of the paper is organized as follows. In Section 2, the dimensionless Vlasov-Maxwell system under some characteristic scales and the derivation of an asymptotic model will be presented. The verification of preservation for some good features as well as the existence of weak solutions for the asymptotic model will also be given. The numerical scheme will be briefly described in Section 3 and followed by some numerical examples in Section 4. Conclusions and our future work are in Section 5.

2. Mathematical modeling

In this paper, we start from the Vlasov equation for each species of ions and electrons,

$$\partial_t f_s \,+\, \mathbf{v}\cdot\nabla_{\mathbf{x}} f_s \,+\, \frac{q_s}{m_s}\Big(\mathbf{E} \,+\, \mathbf{v}\times(\mathbf{B}+\mathbf{B}_{ext})\Big)\cdot\nabla_{\mathbf{v}} f_s \,=\, 0, \quad s=i,\, e, \tag{2.1}$$

where $f_s \equiv f_s(t,\mathbf{x},\mathbf{v})$ is the distribution function, m_s and q_s are the mass and charge, with $s=i,\,e$ for the ions and electrons respectively. Here we assume that the ions have an opposite charge to the electrons $q_i = e = -q_e$ and consider a given large magnetic field $\mathbf{B}_{ext}$, as well as self-consistent electromagnetic fields $\mathbf{E}$ and $\mathbf{B}$, which satisfy the Maxwell equations

$$\begin{cases} \nabla_{\mathbf{x}}\times\mathbf{E} \,=\, -\partial_t\mathbf{B}, \\ \nabla_{\mathbf{x}}\times\mathbf{B} \,=\, \dfrac{1}{c^2}\,\partial_t\mathbf{E} \,+\, \mu_0\,\mathbf{J}, \\ \nabla_{\mathbf{x}}\cdot\mathbf{E} \,=\, \dfrac{\rho}{\varepsilon_0}, \\ \nabla_{\mathbf{x}}\cdot\mathbf{B} \,=\, 0, \end{cases} \tag{2.2}$$

where c is the speed of light, μ_0 is the vacuum permeability, ε_0 is the vacuum permittivity and $\mu_0\varepsilon_0 = 1/c^2$. The density n_s, average velocity $\mathbf{u}_s$ are related to the distribution function f_s by

$$n_s \,=\, \int_{\mathbb{R}^3} f_s d\mathbf{v}, \quad n_s\mathbf{u}_s \,=\, \int_{\mathbb{R}^3} f_s\mathbf{v}d\mathbf{v},$$

hence we define the total charge density ρ and total current density $\mathbf{J}$ as $\rho \,=\, e\,(n_i - n_e)$ and $\mathbf{J} \,=\, e\,(n_i\,\mathbf{u}_i - n_e\,\mathbf{u}_e)$.

2.1. Rescaling of the Vlasov-Maxwell system.

In the following we will derive an appropriate dimensionless scaling for (2.1) and (2.2) by introducing a set of characteristic scales.

We assume that the plasma is such that the characteristic density and temperature of ions and electrons are of the same order, that is,

$$\overline{n} := \overline{n}_i \,=\, \overline{n}_e, \quad \overline{T} := \overline{T}_i \,=\, \overline{T}_e. \tag{2.3}$$

We choose to perform a scaling with respect to the ions. On the one hand, we set the characteristic velocity scale $\overline{v}$ as the thermal velocity corresponding to ions,

$$\overline{v} \,:=\, \left(\frac{\kappa_{\mathcal{B}}\overline{T}}{m_i}\right)^{1/2},$$

where $\kappa_{\mathcal{B}}$ is the Boltzmann constant. Then we define the characteristic length scale of $\overline{x}$ given by the Debye length, which is the same for ions and electrons

$$\overline{x} \,:=\, \lambda_D \,=\, \left(\frac{\varepsilon_0\kappa_{\mathcal{B}}\overline{T}}{\overline{n}e^2}\right)^{1/2}.$$

It allows to define a first time scale corresponding to the plasma frequency of ions $\omega_p := \overline{v}/\overline{x}$.

Finally, the characteristic magnitude of the electric field $\mathbf{E}$ can be expressed from $\overline{n}$ and $\overline{x}$ by

$$\overline{E} \,:=\, \frac{e\,\overline{n}\,\overline{x}}{\varepsilon_0},$$

hence the characteristic magnitude of the self-consistent magnetic field $\mathbf{B}$, which is denoted by $\overline{B}$, is related to the scale of the electric field by $\overline{E} = \overline{v}\,\overline{B}$.

On the other hand, by denoting $\overline{B}_{ext}$ the characteristic magnitude of the given magnetic field $\mathbf{B}_{ext}$, we define the cyclotron frequency corresponding to ions by

$$\omega_c \,:=\, \frac{e\overline{B}_{ext}}{m_i}$$

and ω_c^{-1} corresponds to a second time scale.

With the above introduced scales, we define the scaled variables as

$$\mathbf{v}' = \frac{\mathbf{v}}{\overline{v}}, \quad \mathbf{x}' = \frac{\mathbf{x}}{\overline{x}}, \quad t' = \frac{t}{\bar{t}},$$

and the electromagnetic field as

$$\mathbf{E}'(t', \mathbf{x}') = \frac{\mathbf{E}(t, \mathbf{x})}{\overline{E}}, \quad \mathbf{B}(t', \mathbf{x}') = \frac{\mathbf{B}(t, \mathbf{x})}{\overline{B}}, \quad \mathbf{B}'_{ext}(t', \mathbf{x}') = \frac{\mathbf{B}_{ext}(t, \mathbf{x})}{\overline{B}_{ext}}.$$

Furthermore, for each species, we define the characteristic velocity and subsequently, by letting $\overline{f} = \overline{n}/\overline{v}^3$,

$$f'_s(t', \mathbf{x}', \mathbf{v}') = \frac{f_s(t, \mathbf{x}, \mathbf{v})}{\overline{f}}, \quad s = i, e.$$

Inserting all these new variables into (2.1), dividing by ω_p and dropping the primes for clarity, we obtain the following dimensionless Vlasov equation

$$\left\{ \begin{array}{l} \dfrac{1}{\omega_p \bar{t}}\, \partial_t f_i + \mathbf{v}\cdot\nabla_{\mathbf{x}} f_i + \left(\mathbf{E} + \mathbf{v}\times\mathbf{B} + \dfrac{\omega_c}{\omega_p}\,\mathbf{v}\times\mathbf{B}_{ext}\right)\cdot\nabla_{\mathbf{v}} f_i = 0, \\ \dfrac{1}{\omega_p \bar{t}}\, \partial_t f_e + \mathbf{v}\cdot\nabla_{\mathbf{x}} f_e - \dfrac{m_i}{m_e}\left(\mathbf{E} + \mathbf{v}\times\mathbf{B} + \dfrac{\omega_c}{\omega_p}\,\mathbf{v}\times\mathbf{B}_{ext}\right)\cdot\nabla_{\mathbf{v}} f_e = 0, \end{array} \right. \tag{2.4}$$

while the dimensionless Maxwell equations (2.2) are scaled according to the plasma frequency of ions,

$$\left\{ \begin{array}{l} \nabla_{\mathbf{x}}\times\mathbf{E} = -\dfrac{1}{\omega_p \bar{t}}\,\partial_t\mathbf{B}, \\ \nabla_{\mathbf{x}}\times\mathbf{B} = \mathrm{Ma}^2\left(\dfrac{1}{\omega_p \bar{t}}\,\partial_t\mathbf{E} + \mathbf{J}\right), \\ \nabla_{\mathbf{x}}\cdot\mathbf{E} = \rho, \\ \nabla_{\mathbf{x}}\cdot\mathbf{B} = 0, \end{array} \right. \tag{2.5}$$

where $\mathrm{Ma} = \overline{v}/c$ is the Mach number and

$$\rho = n_i - n_e, \quad \mathbf{J} = n_i\,\mathbf{u}_i - n_e\,\mathbf{u}_e\,. \tag{2.6}$$

To consider an asymptotic limit, we introduce a dimensionless cyclotron period of ions

$$\varepsilon := \frac{\omega_p}{\omega_c},$$

where ε is a small parameter and study the long time asymptotic, that is, $\varepsilon = 1/(\omega_p\bar{t}) \ll 1$. We also denote by α the mass ratio between electrons and ions

$$\alpha := \frac{m_e}{m_i}.$$

Under these two scalings, the Vlasov equation (2.4) takes the form

$$\left\{ \begin{array}{l} \varepsilon\,\partial_t f_i + \mathbf{v}\cdot\nabla_{\mathbf{x}} f_i + \left(\mathbf{E} + \mathbf{v}\times\mathbf{B} + \dfrac{1}{\varepsilon}\mathbf{v}\times\mathbf{B}_{ext}\right)\cdot\nabla_{\mathbf{v}} f_i = 0, \\ \varepsilon\,\partial_t f_e + \mathbf{v}\cdot\nabla_{\mathbf{x}} f_e - \dfrac{1}{\alpha}\left(\mathbf{E} + \mathbf{v}\times\mathbf{B} + \dfrac{1}{\varepsilon}\mathbf{v}\times\mathbf{B}_{ext}\right)\cdot\nabla_{\mathbf{v}} f_e = 0 \end{array} \right. \tag{2.7}$$

and the Maxwell equations (2.5) are

$$\begin{cases} \nabla_{\mathbf{x}} \times \mathbf{E} \;=\; -\varepsilon\, \partial_t \mathbf{B}, \\ \nabla_{\mathbf{x}} \times \mathbf{B} \;=\; \mathrm{Ma}^2\, (\varepsilon\, \partial_t \mathbf{E} + \mathbf{J}), \\ \nabla_{\mathbf{x}} \cdot \mathbf{E} \;=\; \rho, \\ \nabla_{\mathbf{x}} \cdot \mathbf{B} \;=\; 0, \end{cases} \tag{2.8}$$

with ρ and $\mathbf{J}$ given by (2.6).

2.2. **Asymptotic limit of the Vlasov-Maxwell system.** To derive an asymptotic model from (2.7)-(2.8), let us set our assumptions

Assumption 2.1. Consider $\mathbf{\Omega} \subset \mathbb{R}^2$ and $D = \Omega \times [0, L_z]$, the external magnetic filed only applies in the z-direction

$$\mathbf{B}_{ext} = (0, 0, 1)^t.$$

For simplicity we consider here periodic boundary conditions in space for the distribution function and the electromagnetic field.

Assumption 2.2. The plasma is homogeneous in the direction parallel to the applied magnetic field. Hence, the distribution functions f_i and f_e do not depend on z.

For any $\mathbf{x} = (x, y, z)^t \in \mathbb{R}^3$, we decompose it as $\mathbf{x} = \mathbf{x}_\perp + \mathbf{x}_\parallel$ according to the orthogonal and parallel directions to the external magnetic field $\mathbf{B}_{ext}$, that is, $\mathbf{x}_\perp = (x, y, 0)^t$ and $\mathbf{x}_\parallel = (0, 0, z)$. In the same manner, the velocity is $\mathbf{v} = \mathbf{v}_\perp + \mathbf{v}_\parallel \in \mathbb{R}^3$ with $\mathbf{v}_\perp = (v_x, v_y, 0)^t$ and $\mathbf{v}_\parallel = (0, 0, v_z)$. Under these assumptions and notations, the Vlasov equation (2.7) can be written in the following form,

$$\begin{cases} \varepsilon\, \partial_t f_i \,+\, \mathbf{v} \cdot \nabla_{\mathbf{x}} f_i \,+\, (\mathbf{E} + \mathbf{v} \times \mathbf{B}) \cdot \nabla_{\mathbf{v}} f_i \,+\, \dfrac{\mathbf{v}^\perp}{\varepsilon} \cdot \nabla_{\mathbf{v}} f_i \;=\; 0, \\ \varepsilon\, \partial_t f_e \,+\, \mathbf{v} \cdot \nabla_{\mathbf{x}} f_e \,-\, \dfrac{1}{\alpha} (\mathbf{E} + \mathbf{v} \times \mathbf{B}) \cdot \nabla_{\mathbf{v}} f_e \,-\, \dfrac{\mathbf{v}^\perp}{\varepsilon\, \alpha} \cdot \nabla_{\mathbf{v}} f_e \;=\; 0, \end{cases} \tag{2.9}$$

where $\mathbf{v}^\perp = (v_y, -v_x, 0)$ for any $\mathbf{v} \in \mathbb{R}^3$.

Now we reformulate the Maxwell equations using Assumption 2.2. Here and after, we will drop the subindex $\mathbf{x}$ for spatial derivatives of macroscopic quantities which do not depend on $\mathbf{v}$, such as $\mathbf{E}$ and $\mathbf{B}$ and their related quantities, for clarity. On the one hand, from the divergence free condition of (2.8), we can write $\mathbf{B} = \nabla_{\mathbf{x}} \times \mathbf{A}$, where $\mathbf{A}$ is a magnetic potential verifying the Coulomb's gauge

$$\nabla_{\mathbf{x}} \cdot \mathbf{A} \;=\; 0.$$

On the other hand, the electric field $\mathbf{E}$ is split into a longitudinal part and a transversal part $\mathbf{E} = \mathbf{E}_L + \mathbf{E}_T$, with

$$\begin{cases} \nabla_{\mathbf{x}} \times \mathbf{E}_L = 0, \\ \nabla_{\mathbf{x}} \cdot \mathbf{E}_T = 0. \end{cases}$$

From (2.8) it is easy to see that $\mathbf{E}_L = -\nabla_{\mathbf{x}} \Phi$, where the electrical potential Φ is a solution to the Poisson's equation,

$$-\Delta_{\mathbf{x}} \Phi = \rho. \tag{2.10}$$

Then, from (2.8) we get that

$$\nabla_{\mathbf{x}} \times \mathbf{E}_T \;=\; -\partial_t \mathbf{B} \;=\; -\varepsilon\, \nabla_{\mathbf{x}} \times (\partial_t \mathbf{A}),$$

hence using the uniqueness of the decomposition for given boundary conditions, we necessarily have, assuming periodic boundary conditions, that $\mathbf{E}_T = -\varepsilon \partial_t \mathbf{A}$ and the electric field $\mathbf{E}$ is given by

$$\mathbf{E} \;=\; -\nabla_{\mathbf{x}} \Phi \,-\, \varepsilon \partial_t \mathbf{A}. \tag{2.11}$$

Furthermore, the second equation in (2.8) gives the equation satisfied by the potential $\mathbf{A}$, that is,

$$(\varepsilon\,\mathrm{Ma})^2\,\partial_{tt}^2\mathbf{A} \,-\, \Delta_{\mathbf{x}}\mathbf{A} \;=\; \mathrm{Ma}^2\,(\mathbf{J} \,-\, \varepsilon\,\partial_t\nabla_{\mathbf{x}}\Phi)\,. \tag{2.12}$$

Gathering (2.10)-(2.12), we finally have $\mathbf{E} = -\nabla_{\mathbf{x}}\Phi - \varepsilon\,\partial_t\mathbf{A}$ and $\mathbf{B} = \nabla_{\mathbf{x}}\times\mathbf{A}$,

$$\left\{\begin{array}{l} (\varepsilon\,\mathrm{Ma})^2\,\partial_{tt}^2\mathbf{A} \,-\, \Delta_{\mathbf{x}}\mathbf{A} \;=\; \mathrm{Ma}^2\,(\mathbf{J} \,-\, \varepsilon\,\partial_t\nabla_{\mathbf{x}}\Phi)\,, \\ \\ -\Delta_{\mathbf{x}}\Phi \;=\; \rho. \end{array}\right. \tag{2.13}$$

Now we remind the basic properties of the solution to (2.9) and (2.13)

Proposition 2.3. We consider that Assumptions 2.1 and 2.2 are verified and $(f_i^\varepsilon, f_e^\varepsilon, \Phi^\varepsilon, \mathbf{A}^\varepsilon)_{\varepsilon>0}$ is a solution to (2.9) and (2.13). Then we have for all $t \geq 0$,

$$\|f_s^\varepsilon(t)\|_{L^p} = \|f_s^\varepsilon(0)\|_{L^p}, \qquad s = i,\, e.$$

Moreover we define the total energy at time $t \geq 0$, as

$$\mathcal{E}^\varepsilon(t) := \int_{\mathbb{T}^2\times\mathbb{R}^3} [f_i^\varepsilon(t) \,+\, \alpha\, f_e^\varepsilon(t)]\;\frac{|\mathbf{v}|^2}{2}\,d\mathbf{x}_\perp\,d\mathbf{v} \,+\, \frac{1}{2}\int_{\mathbb{T}^2}\left[|\nabla_{\mathbf{x}}\Phi|^2 \,+\, \varepsilon|\partial_t\mathbf{A}|^2 \,+\, \frac{1}{\mathrm{Ma}^2}|\nabla_{\mathbf{x}}\times\mathbf{A}|^2\right]\,d\mathbf{x}_\perp,$$

which is conserved for all time $t \geq 0$, $\mathcal{E}^\varepsilon(t) = \mathcal{E}^\varepsilon(0)$.

We now derive the asymptotic limit of (2.9) and (2.13) by letting $\varepsilon \to 0$. We denote the solutions to the above equations (2.9) and (2.13) as $(f_i^\varepsilon, f_e^\varepsilon, \mathbf{A}^\varepsilon, \Phi^\varepsilon)$, and perform Hilbert expansions for $s = i,\, e$

$$\left\{\begin{array}{l} f_s^\varepsilon = f_{s,0} + \varepsilon f_{s,1} + \varepsilon^2 f_{s,2} + \cdots\,, \\ \\ \mathbf{A}^\varepsilon \;=\; \mathbf{A}_0 \,+\, \varepsilon\,\mathbf{A}_1 \,+\cdots\,, \\ \\ \Phi^\varepsilon \;=\; \Phi_0 \,+\, \varepsilon\,\Phi_1 \,+\cdots\,, \end{array}\right. \tag{2.14}$$

correspondingly

$$\mathbf{E}^\varepsilon \;=\; \mathbf{E}_0 \,+\, \varepsilon\,\mathbf{E}_1 \,+\,\cdots\,, \quad \mathbf{B}^\varepsilon \;=\; \mathbf{B}_0 \,+\, \varepsilon\,\mathbf{B}_1 \,+\,\cdots\,.$$

We prove the following asymptotic limit

Theorem 2.4 (Formal expansion)**.** *Consider that Assumptions 2.1 and 2.2 are satisfied. Let $(f_i^\varepsilon, f_e^\varepsilon, \mathbf{A}^\varepsilon, \Phi^\varepsilon)$ be a nonnegative solution to the Vlasov-Maxwell system* (2.9) *and* (2.13) *satisfying (2.14). Then, the leading term $(f_{i,0}, f_{e,0}, \Phi_0, \mathbf{A}_0)$ is such that*

$$\left\{\begin{array}{l} \Phi_0 \equiv \Phi(t,\mathbf{x}), \\ \\ \mathbf{A}_0 \equiv (0,0,A(t,\mathbf{x}))^t. \end{array}\right.$$

Furthermore, we define (F_i, F_e) as

$$F_i(t,\mathbf{x},p_z) \;=\; \frac{1}{2\pi}\int_{\mathbb{R}^2} f_{i,0}(t,\mathbf{x},\mathbf{v})\,dv_x\,dv_y, \quad F_e(t,\mathbf{x},q_z) \;=\; \alpha^{-1}\,\frac{1}{2\pi}\int_{\mathbb{R}^2} f_{e,0}(t,\mathbf{x},\mathbf{v})\,dv_x\,dv_y$$

where $p_z = v_z + A(t,\mathbf{x})$ and $q_z = \alpha\,v_z - A(t,\mathbf{x})$, and the two Hamiltonians

$$\mathcal{H}_i \;=\; \Phi \,+\, \frac{1}{2}\,(A - p_z)^2 \quad \text{and} \quad \mathcal{H}_e \;=\; \Phi \,-\, \frac{1}{2\alpha}\,(q_z + A)^2\,,$$

where (F_i, F_e, Φ, A) is a solution to the following system

$$\left\{\begin{array}{l} \partial_t F_i \,-\, \nabla_{\mathbf{x}}^\perp\mathcal{H}_i\cdot\nabla_{\mathbf{x}}F_i \;=\; 0, \\ \\ \partial_t F_e \,-\, \nabla_{\mathbf{x}}^\perp\mathcal{H}_e\cdot\nabla_{\mathbf{x}}F_e \;=\; 0, \\ \\ -\Delta_{\mathbf{x}}\Phi \;=\; \rho, \\ \\ -\Delta_{\mathbf{x}}A \,+\, Ma^2\,\left(n_i + \dfrac{n_e}{\alpha}\right)\,A \;=\; Ma^2\,\mathcal{J}_z, \end{array}\right. \tag{2.15}$$

and the density n_i and n_e are given by

$$n_s \;=\; \int_{\mathbb{R}} F_s(t,\mathbf{x},r_z)\,dr_z, \quad s=i,\,e, \tag{2.16}$$

hence the charge density is $\rho = n_i - n_e$ and the current density corresponds to

$$\mathcal{J}_z \;=\; \int_{\mathbb{R}} r_z \left(F_i(t,\mathbf{x},r_z) \;-\; \frac{1}{\alpha}\, F_e(t,\mathbf{x},r_z) \right) dr_z, \tag{2.17}$$

where the Mach number $Ma = \overline{v}/c$.

Remark 2.5. Observe that the drift velocity in (2.15) called $\mathbf{E}\times\mathbf{B} = \nabla^{\perp}_{\mathbf{x}}\Phi$ is the same for the two species, since it does not depend on the charge of the particle.

Proof. We first start with the self-consistent electromagnetic fields, we can easily find from (2.13) that $\mathbf{E}_0 \;=\; -\nabla_{\mathbf{x}}\Phi_0$ and $\mathbf{B}_0 \;=\; \nabla_{\mathbf{x}}\times\mathbf{A}_0$ with

$$\begin{cases} -\Delta_{\mathbf{x}}\Phi_0 \;=\; \rho_0, \\ \\ -\Delta_{\mathbf{x}}\mathbf{A}_0 \;=\; \mathrm{Ma}^2\,\mathbf{J}_0, \end{cases} \tag{2.18}$$

and at the next order $\mathbf{E}_1 = -\nabla_{\mathbf{x}}\Phi_1 - \partial_t\mathbf{A}_0$ and $\mathbf{B}_1 = \nabla_{\mathbf{x}}\times\mathbf{A}_1$, with

$$\begin{cases} -\Delta_{\mathbf{x}}\Phi_1 \;=\; \rho_1, \\ \\ -\Delta_{\mathbf{x}}\mathbf{A}_1 \;=\; \mathrm{Ma}^2\,\left(\mathbf{J}_1 \;-\; \partial_t\nabla_{\mathbf{x}}\Phi_0\right), \end{cases} \tag{2.19}$$

where for $k=0,\,1$,

$$\rho_k \;=\; \int_{\mathbb{R}^3} [f_{i,k} \;-\; f_{e,k}]\,d\mathbf{v}\,, \quad \mathbf{J}_k \;=\; \int_{\mathbb{R}^3} \mathbf{v}\;[\,f_{i,k} - f_{e,k}\,]\;d\mathbf{v}.$$

Substituting the Hilbert expansions into (2.9), and comparing the orders of ε, such as $\varepsilon^{-1}, \varepsilon^0$ and ε, we obtain the following three equations for ions:

$$\begin{cases} \mathbf{v}^{\perp}\cdot\nabla_{\mathbf{v}} f_{i,0} \;=\; 0, \\ \\ \mathbf{v}\cdot\nabla_{\mathbf{x}} f_{i,0} + (\mathbf{E}_0 + \mathbf{v}\times\mathbf{B}_0)\cdot\nabla_{\mathbf{v}} f_{i,0} \;=\; -\mathbf{v}^{\perp}\cdot\nabla_{\mathbf{v}} f_{i,1}, \\ \\ \partial_t f_{i,0} + \mathbf{v}\cdot\nabla_{\mathbf{x}} f_{i,1} + (\mathbf{E}_0 + \mathbf{v}\times\mathbf{B}_0)\cdot\nabla_{\mathbf{v}} f_{i,1} + (\mathbf{E}_1 + \mathbf{v}\times\mathbf{B}_1)\cdot\nabla_{\mathbf{v}} f_{i,0} \;=\; -\mathbf{v}^{\perp}\cdot\nabla_{\mathbf{v}} f_{i,2} \end{cases} \tag{2.20}$$

and for electrons:

$$\begin{cases} \mathbf{v}^{\perp}\cdot\nabla_{\mathbf{v}} f_{e,0} \;=\; 0, \\ \\ \alpha\mathbf{v}\cdot\nabla_{\mathbf{x}} f_{e,0} - (\mathbf{E}_0 + \mathbf{v}\times\mathbf{B}_0)\cdot\nabla_{\mathbf{v}} f_{e,0} \;=\; \mathbf{v}^{\perp}\cdot\nabla_{\mathbf{v}} f_{e,1}, \\ \\ \alpha\;(\partial_t f_{e,0} + \mathbf{v}\cdot\nabla_{\mathbf{x}} f_{e,1}) - (\mathbf{E}_0 + \mathbf{v}\times\mathbf{B}_0)\cdot\nabla_{\mathbf{v}} f_{e,1} - (\mathbf{E}_1 + \mathbf{v}\times\mathbf{B}_1)\cdot\nabla_{\mathbf{v}} f_{e,0} \;=\; \mathbf{v}^{\perp}\cdot\nabla_{\mathbf{v}} f_{e,2}. \end{cases} \tag{2.21}$$

We now pass in cylindrical coordinates in velocity $\mathbf{v} = \mathbf{v}_{\perp} + \mathbf{v}_{\parallel}$, with

$$\mathbf{v}_{\perp} \;=\; \omega\,\mathbf{e}_{\omega},$$

where we have set $\omega = |\mathbf{v}_{\perp}|$ and

$$\mathbf{e}_{\omega} = \begin{pmatrix} \cos\theta \\ \sin\theta \\ 0 \end{pmatrix}, \quad \mathbf{e}_{\theta} = \begin{pmatrix} -\sin\theta \\ \cos\theta \\ 0 \end{pmatrix}.$$

Using these notations, we now derive the asymptotic limit according to the orders of ε in (2.20)-(2.21). First the leading order term in (2.20)-(2.21) written in cylindrical coordinates becomes

$$-\partial_{\theta} f_{s,0} = 0, \quad s \;=\; i,\,e,$$

which means that $f_{s,0}$ does not depend on θ, hence from Assumption 2.2, it yields that $f_{s,0} \;\equiv\; f_{s,0}(t,\mathbf{x}_{\perp},\omega,v_z)$.

As a consequence, the current density is such that

$$(n_s \mathbf{u}_{s,0})_\perp := \int_{\mathbb{R}^3} \mathbf{v}_\perp f_{s,0}\, d\mathbf{v} = \int_{\mathbb{R}} \int_0^\infty f_{s,0} \left(\int_0^{2\pi} \mathbf{e}_\omega d\theta \right) \omega^2\, d\omega\, dv_z = \mathbf{0},$$

which implies that only the third component of the total current density $\mathbf{J}_0$ might be nonzero and therefore only the third component of $\mathbf{A}_0$ in (2.18) might be nonzero, that is, $\mathbf{A}_0 = (0, 0, A_0)$ is a solution to the Poisson's equation with the source term $\mathbf{J}_0 = (0, 0, j_z)$

$$-\Delta_{\mathbf{x}} A_0 = \mathrm{Ma}^2\, j_z,$$

hence from $\mathbf{B}_0 = \nabla_{\mathbf{x}} \times \mathbf{A}_0$, it yields that $\mathbf{B}_0 = \nabla_{\mathbf{x}}^\perp A_0$ and particularly $B_{0,z} = 0$.

Finally, since the electric field $\mathbf{E}_0 = -\nabla_{\mathbf{x}} \Phi_0$ and from Assumption 2.2, we also have that $E_{0,z} = 0$.

Now we treat the zeroth order term in (2.20)-(2.21) and use the cylindrical coordinates in the velocity variable, it gives

$$\partial_\theta f_{i,1} = \mathbf{e}_\omega \cdot \mathbf{G}_{i,0}, \qquad \partial_\theta f_{e,1} = \mathbf{e}_\omega \cdot \mathbf{G}_{e,0}, \tag{2.22}$$

with

$$\begin{cases} \mathbf{G}_{i,0} = +\big(\omega\, \nabla_{\mathbf{x}} f_{i,0} - (\nabla_{\mathbf{x}} \Phi_0 - v_z \nabla_{\mathbf{x}} A_0)\, \partial_\omega f_{i,0} - \omega\, \nabla_{\mathbf{x}} A_0\, \partial_{v_z} f_{i,0} \big), \\ \mathbf{G}_{e,0} = -\big(\alpha\, \omega\, \nabla_{\mathbf{x}} f_{e,0} + (\nabla_{\mathbf{x}} \Phi_0 - v_z \nabla_{\mathbf{x}} A_0)\, \partial_\omega f_{e,0} + \omega\, \nabla_{\mathbf{x}} A_0\, \partial_{v_z} f_{e,0} \big). \end{cases} \tag{2.23}$$

First notice that $\mathbf{G}_{e,0}$ and $\mathbf{G}_{i,0}$ do not depend on $\theta \in (0, 2\pi)$ since f_0 does not depend on θ and

$$\int_0^{2\pi} \mathbf{e}_\omega\, d\theta = \mathbf{0},$$

then the solvability condition of (2.22) is automatically satisfied and after integration in θ, we obtain f_1 as,

$$\begin{cases} f_{i,1}(t, \mathbf{x}_\perp, \omega, \theta, v_z) = -\mathbf{e}_\theta \cdot \mathbf{G}_{i,0}(t, \mathbf{x}_\perp, \omega, v_z) + h_i(t, \mathbf{x}_\perp, \omega, v_z), \\ f_{e,1}(t, \mathbf{x}_\perp, \omega, \theta, v_z) = -\mathbf{e}_\theta \cdot \mathbf{G}_{e,0}(t, \mathbf{x}_\perp, \omega, v_z) + h_e(t, \mathbf{x}_\perp, \omega, v_z), \end{cases} \tag{2.24}$$

where h_i and h_e are arbitrary functions which do not depend on θ.

Now we focus on the first order with respect to ε in (2.20)-(2.21). Similarly, from the periodic boundary condition in $\theta \in (0, 2\pi)$, we have the following solvability condition

$$\frac{1}{2\pi} \int_0^{2\pi} \partial_\theta f_{s,2}\, d\theta = 0, \quad s = i,\, e.$$

Therefore, we have

$$\begin{cases} \partial_t f_{i,0} + \dfrac{1}{2\pi} \displaystyle\int_0^{2\pi} \Big(\mathbf{v} \cdot \nabla_{\mathbf{x}} f_{i,1} + (\mathbf{E}_0 + \mathbf{v} \times \mathbf{B}_0) \cdot \nabla_{\mathbf{v}} f_{i,1} + (\mathbf{E}_1 + \mathbf{v} \times \mathbf{B}_1) \cdot \nabla_{\mathbf{v}} f_{i,0} \Big) d\theta = 0, \\ \alpha \partial_t f_{e,0} + \dfrac{1}{2\pi} \displaystyle\int_0^{2\pi} \Big(\alpha \mathbf{v} \cdot \nabla_{\mathbf{x}} f_{e,1} - (\mathbf{E}_0 + \mathbf{v} \times \mathbf{B}_0) \cdot \nabla_{\mathbf{v}} f_{e,1} - (\mathbf{E}_1 + \mathbf{v} \times \mathbf{B}_1) \cdot \nabla_{\mathbf{v}} f_{e,0} \Big) d\theta = 0. \end{cases} \tag{2.25}$$

Each integral term can be explicitly calculated by substituting $f_{i,1}$ and $f_{e,1}$ from (2.24). On the one hand, observing that

$$\begin{cases} \partial_\omega f_{s,1} = -\mathbf{e}_\theta \cdot \partial_\omega \mathbf{G}_{s,0} + \partial_\omega h_s, \ s = i,\, e\,, \\ \partial_\theta f_{s,1} = \mathbf{e}_\omega \cdot \mathbf{G}_{s,0}, \ s = i,\, e\,, \end{cases}$$

it yields for $s = i,\, e$,

$$\frac{1}{2\pi} \int_0^{2\pi} \mathbf{v} \cdot \nabla_{\mathbf{x}} f_{s,1}\, d\theta = -\frac{\omega}{2} \nabla_{\mathbf{x}} \cdot \mathbf{G}_{s,0}^\perp. \tag{2.26}$$

On the other hand, the same kind of computation leads to for $s = i,\, e$,

$$\frac{1}{2\pi}\int_0^{2\pi} (\mathbf{E}_0 + \mathbf{v}\times\mathbf{B}_0)\cdot\nabla_{\mathbf{v}} f_{s,1}\, d\theta = -\frac{1}{2}\left[\frac{(\mathbf{E}_0 + v_z\nabla_{\mathbf{x}}A_0)}{\omega}\cdot\partial_\omega\left(\omega\mathbf{G}^\perp_{s,0}\right) - \omega\nabla_{\mathbf{x}}A_0\cdot\partial_{v_z}\mathbf{G}^\perp_{s,0}\right]. \tag{2.27}$$

Finally since $f_{s,0}$ does not depend on $\theta\in(0,2\pi)$ and the electric field does not depend on z, the last term in (2.25) only gives

$$\frac{1}{2\pi}\int_0^{2\pi} (\mathbf{E}_1 + \mathbf{v}\times\mathbf{B}_1)\cdot\nabla_{\mathbf{v}} f_{s,0}\, d\theta = -\partial_t A_0\,\partial_{v_z} f_{s,0}, \quad s\,=\,i\,,e. \tag{2.28}$$

Gathering (2.26)-(2.28), and recalling that $\mathbf{E}_0 = -\nabla_{\mathbf{x}}\Phi_0$, we get for the distribution function $f_{i,0}$,

$$\begin{aligned}\partial_t f_{i,0} \,-\, \frac{\omega}{2}\nabla_{\mathbf{x}}\cdot\mathbf{G}^\perp_{i,0} \;\;+\;\; \frac{1}{2}\left(\frac{\nabla_{\mathbf{x}}\left(\Phi_0 - v_z A_0\right)}{\omega}\cdot\partial_\omega\left(\omega\,\mathbf{G}^\perp_{i,0}\right) + \omega\nabla_{\mathbf{x}}A_0\cdot\partial_{v_z}\mathbf{G}^\perp_{i,0}\right)\\ -\;\; \partial_t A_0\,\partial_{v_z} f_{i,0} \;=\; 0.\end{aligned}$$

and for the distribution function $f_{e,0}$,

$$\begin{aligned}\alpha\left(\partial_t f_{e,0} \,-\, \frac{\omega}{2}\nabla_{\mathbf{x}}\cdot\mathbf{G}^\perp_{e,0}\right) \;\;-\;\; \frac{1}{2}\left(\frac{\nabla_{\mathbf{x}}\left(\Phi_0 - v_z A_0\right)}{\omega}\cdot\partial_\omega(\omega\,\mathbf{G}^\perp_{e,0}) + \omega\nabla_{\mathbf{x}}A_0\cdot\partial_{v_z}\mathbf{G}^\perp_{e,0}\right)\\ +\;\; \partial_t A_0\,\partial_{v_z} f_{e,0} \;=\; 0.\end{aligned}$$

Using the definition of $\mathbf{G}_{s,0}$ for $s = i, e$ in (2.23) and after some calculations, it finally yields that

$$\begin{cases} \partial_t f_{i,0} - \nabla^\perp_{\mathbf{x}}\left(\Phi_0 - v_z A_0\right)\cdot\nabla_{\mathbf{x}} f_{i,0} \,-\, \left(\nabla_{\mathbf{x}}\Phi_0\cdot\nabla^\perp_{\mathbf{x}}A_0 + \partial_t A_0\right)\partial_{v_z} f_{i,0} \;=\; 0,\\[2ex] \alpha\left(\partial_t f_{e,0} - \nabla^\perp_{\mathbf{x}}\left(\Phi_0 - v_z A_0\right)\cdot\nabla_{\mathbf{x}} f_{e,0}\right) + \left(\nabla_{\mathbf{x}}\Phi_0\cdot\nabla^\perp_{\mathbf{x}}A_0 + \partial_t A_0\right)\partial_{v_z} f_{e,0} \;=\; 0. \end{cases} \tag{2.29}$$

Observing that this equation does not explicitly depend on ω, we define

$$F_{s,0}(t,\mathbf{x}_\perp, v_z) \;:=\; \frac{1}{2\pi}\int_{\mathbb{R}^2} f_{s,0}(t,\mathbf{x}_\perp,\mathbf{v})\, dv_x\, dv_y, \quad s\,=\,i,\,e\,.$$

Multiplying (2.29) by ω and integrating with respect to ω, we get

$$\begin{cases} \partial_t F_{i,0} \,-\, \nabla^\perp_{\mathbf{x}}\left(\Phi_0 - v_z A_0\right)\cdot\nabla_{\mathbf{x}} F_{i,0} \,-\, \left(\nabla_{\mathbf{x}}\Phi_0\cdot\nabla^\perp_{\mathbf{x}}A_0 + \partial_t A_0\right)\partial_{v_z} F_{i,0} \;=\; 0,\\[2ex] \alpha\left(\partial_t F_{e,0} \,-\, \nabla^\perp_{\mathbf{x}}\left(\Phi_0 - v_z A_0\right)\cdot\nabla_{\mathbf{x}} F_{e,0}\right) + \left(\nabla_{\mathbf{x}}\Phi_0\cdot\nabla^\perp_{\mathbf{x}}A_0 + \partial_t A_0\right)\partial_{v_z} F_{e,0} \;=\; 0. \end{cases} \tag{2.30}$$

This last equation can be reformulated to remove the time derivative of A_0 in the velocity field. To this aim, we introduce a new variable for $p_z \,=\, v_z \,+\, A_0(t,\mathbf{x})$ in $F_{i,0}$ and $q_z \,=\, \alpha\, v_z \,-\, A_0(t,\mathbf{x})$ in $F_{e,0}$ and perform a change of variable in velocity

$$F_i(t,\mathbf{x}_\perp,p_z) \,=\, F_{i,0}(t,\mathbf{x}_\perp,v_z), \quad F_e(t,\mathbf{x}_\perp,q_z) \,=\, \alpha^{-1}\, F_{e,0}(t,\mathbf{x}_\perp,v_z).$$

From now on, we will use $\Phi(t,\mathbf{x})$ and $A(t,\mathbf{x})$ in short of $\Phi_0(t,\mathbf{x})$ and $A_0(t,\mathbf{x})$ respectively. Hence (2.30) now becomes

$$\begin{cases} \partial_t F_i \,-\, \nabla^\perp_{\mathbf{x}}\mathcal{H}_i\cdot\nabla_{\mathbf{x}} F_i \;=\; 0,\\[2ex] \partial_t F_e \,-\, \nabla^\perp_{\mathbf{x}}\mathcal{H}_e\cdot\nabla_{\mathbf{x}} F_e \;=\; 0, \end{cases}$$

with

$$\mathcal{H}_i \,=\, \Phi + \frac{1}{2}\left(A - p_z\right)^2 \quad \text{and} \quad \mathcal{H}_e \,=\, \Phi \,-\, \frac{1}{2\alpha}\left(A + q_z\right)^2,$$

where the charge density is always given by $\rho = n_i - n_e$, whereas the current density is now given by

$$j_z \,=\, \mathcal{J}_z \,-\, \left(n_i + \frac{n_e}{\alpha}\right) A,$$

where (n_i, n_e) and $\mathcal{J}_z$ are respectively defined in (2.16) and (2.17). Finally, the potentials (Φ, A) are now solutions to

$$\begin{cases} -\Delta_{\mathbf{x}}\Phi \;=\; \rho, \\ \\ -\Delta_{\mathbf{x}} A \,+\, \mathrm{Ma}^2 \left(n_i + \dfrac{n_e}{\alpha}\right) A \,=\, \mathrm{Ma}^2 \mathcal{J}_z, \end{cases}$$

where $\mathrm{Ma} = \overline{v}/c$ is the Mach number. □

2.3. **Weak solutions for the asymptotic model.** First notice that the asymptotic model (2.15) is now two dimensional in space since we assume that the plasma is homogeneous in the parallel direction to the external magnetic field and one dimensional in moment since we have averaged in the orthogonal direction to the external magnetic field.

To simplify the presentation, from now on $\mathbf{x}$ represents the orthogonal part of $\mathbf{x}_\perp = (x, y, 0)$ with $(x, y) \in \Omega$.

For the sake of simplicity in the analysis we have only considered periodic boundary conditions in space, for $\mathbf{x} \in \Omega := (0, L_x) \times (0, L_y)$,

$$\begin{cases} \Phi(t, x + L_x, y) = \Phi(t, x, y), \quad \Phi(t, x, y + L_y) = \Phi(t, x, y), \\ \\ A(t, x + L_x, y) = A(t, x, y), \quad A(t, x, y + L_y) = A(t, x, y), \\ \\ F_i(t, x + L_x, y, p_z) = F_i(t, x, y, p_z), \quad F_i(t, x, y + L_y, p_z) = F_i(t, x, y, p_z),\ p_z \in \mathbb{R}, \\ \\ F_e(t, x + L_x, y, q_z) = F_e(t, x, y, q_z), \quad F_e(t, x, y + L_y, q_z) = F_e(t, x, y, q_z),\ q_z \in \mathbb{R}. \end{cases} \tag{2.31}$$

But other kinds of boundary conditions may be treated for the asymptotic model as homogeneous Dirichlet boundary conditions for the potential Φ and A

$$\Phi(t, \mathbf{x}) = 0, \quad A(t, \mathbf{x}) = 0, \quad \mathbf{x} \in \partial\Omega. \tag{2.32}$$

Then let us review the main features of the asymptotic model (2.15), which make this mathematical model consistent with the initial Vlasov-Maxwell model (2.9) and (2.13).

Proposition 2.6. Consider a solution to the asymptotic model (2.15) with the boundary conditions (2.31), or (2.32), or a combination of both, then it satisfies

- the flow remains incompressible ;
- for any $m > 1$, we have conservation of moments in velocity, for any time $t \geq 0$,

$$\int_{\Omega\times\mathbb{R}} |r_z|^m F_s(t, \mathbf{x}, r_z)\, dr_z\, d\mathbf{x} = \int_{\Omega\times\mathbb{R}} |r_z|^m F_s(0, \mathbf{x}, r_z)\, dr_z\, d\mathbf{x}\,, \quad s \,=\, i,\, e\,; \tag{2.33}$$

- for any continuous function $\phi : \mathbb{R} \mapsto \mathbb{R}$, we have for any time $t \geq 0$,

$$\int_\Omega \int_{\mathbb{R}} \phi(F_s(t, \mathbf{x}, r_z)) d\mathbf{x}\, dr_z \;=\; \int_\Omega \int_{\mathbb{R}} \phi(F_s(0, \mathbf{x}, r_z)) d\mathbf{x}\, dr_z\,, \quad s \,=\, i,\, e\,; \tag{2.34}$$

- the total energy defined by

$$\mathcal{E}(t) \,:=\, \int_{\mathbb{R}} \int_{\mathbf{\Omega}} \frac{|r_z - A|^2}{2} F_i \,+\, \frac{|r_z + A|^2}{2\alpha} F_e d\mathbf{x}\, dr_z \,+\, \frac{1}{2} \int_{\mathbf{\Omega}} |\nabla_{\mathbf{x}}\Phi|^2 + \frac{1}{\mathrm{Ma}^2} |\nabla_{\mathbf{x}} A|^2 \, d\mathbf{x}, \tag{2.35}$$

  is conserved for all time $t \geq 0$.

Proof. The velocity field in (2.15) can be written as

$$\mathbf{U}_s(t, \mathbf{x}, p_z) = -\nabla_{\mathbf{x}}^\perp \mathcal{H}_s, \quad s = e,\, i,$$

hence $\nabla_{\mathbf{x}} \cdot \mathbf{U}_s = 0$ is automatically satisfied and the flow is incompressible.

Then observing that the variable $r_z \in \mathbb{R}$ only appears as a parameter in the equation, we prove the conservation of moments with respect to r_z : for any $m > 1$ we have for $s = i,\, e$,

$$\int_{\Omega\times\mathbb{R}} |r_z|^m F_s(t, \mathbf{x}, r_z)\, dr_z\, d\mathbf{x} = \int_{\Omega\times\mathbb{R}} |r_z|^m F(0, \mathbf{x}, r_z)\, dr_z\, d\mathbf{x}\,.$$

For a given smooth function $\phi : \mathbb{R} \mapsto \mathbb{R}$ and $s = i, e$, if we multiply the first equation in (2.15) by $\phi'(F_s)$, it becomes

$$\partial_t \phi(F_s) + \nabla_{\mathbf{x}} \cdot (\mathbf{U}_s \, \phi(F_s)) = 0.$$

Integrating the above equation in space $\mathbf{\Omega}$ we obtain

$$\frac{\partial}{\partial t} \int_{\mathbf{\Omega}} \phi(F_s) d\mathbf{x} = - \int_{\partial\Omega} \phi(F_s) \, \mathbf{U}_s(t, \mathbf{x}, r_z) \cdot \nu_{\mathbf{x}} d\sigma_{\mathbf{x}},$$

where $\nu_{\mathbf{x}}$ is the outward normal to $\partial\Omega$ at $\mathbf{x}$. Now for periodic boundary conditions (2.31), the right hand side is obviously zero, and for homogeneous Dirichlet boundary conditions (2.32), we observe that the tangential derivatives verify $\nabla_{\mathbf{x}}\Phi \cdot \tau_{\mathbf{x}} = \nabla_{\mathbf{x}} A \cdot \tau_{\mathbf{x}} = 0$, where $\tau_{\mathbf{x}}$ is the tangential vector to $\partial\Omega$ at $\mathbf{x}$. Hence since

$$\mathbf{U}_s \cdot \nu_{\mathbf{x}} = 0, \quad \text{on } \mathbf{x} \in \partial\Omega,$$

the right hand side is also zero in that case. Finally a further integration on r_z shows that

$$\frac{d}{dt} \int_{\mathbf{\Omega}} \int_{r_z} \phi(F_s) dr_z d\mathbf{x} = 0 \tag{2.36}$$

or

$$\int_{\mathbf{\Omega}} \int_{p_z} \phi(F_s(t)) dr_z d\mathbf{x} = \int_{\mathbf{\Omega}} \int_{\mathbb{R}} \phi(F_s(0)) dr_z d\mathbf{x}, \quad t \geq 0.$$

Notice that this result still holds true when ϕ is only continuous. Taking $\phi(F) = F$, it ensures the conservation of mass, $\phi(F_s) = \max(0, F_s)$ gives the non-negativity of the distribution function for nonnegative initial datum, while $\phi(F_s) = F_s^p$ for $1 \leq p < \infty$, it yields the conservation of L^p norm.

Now let us show the conservation of total energy. On the one hand, we multiply the equation on F_i by $\mathcal{H}_i$ and the one on F_e by $\mathcal{H}_e$, it gives after a simple integration by part and using the appropriate boundary conditions (2.31) or (2.32),

$$\int_{\mathbf{\Omega}\times\mathbb{R}} \mathcal{H}_i \, \partial_t F_i \; + \; \mathcal{H}_e \, \partial_t F_e \, d\mathbf{x} \, dr_z \; = \; 0.$$

or

$$\int_{\mathbf{\Omega}\times\mathbb{R}} \frac{(A - r_z)^2}{2} \, \partial_t F_i \; + \; \frac{(A + r_z)^2}{2\alpha} \, \partial_t F_e \, d\mathbf{x} \, dr_z \; + \int_{\mathbf{\Omega}\times\mathbb{R}} \partial_t (n_i - n_e) \, \Phi \, d\mathbf{x} \; = \; 0. \tag{2.37}$$

The first and second terms in the latter equality can be written as

$$\begin{cases} \mathcal{I}_1 := \displaystyle\int_{\mathbf{\Omega}\times\mathbb{R}} \frac{(A - r_z)^2}{2} \, \partial_t F_i \, d\mathbf{x} \, dr_z = \frac{d}{dt} \int_{\mathbf{\Omega}\times\mathbb{R}} \frac{(A - r_z)^2}{2} \, F_i \, d\mathbf{x} \, dr_z \; - \; \int_{\mathbf{\Omega}} (n_i A - \; n_i \, \mathbf{u}_i) \, \partial_t A \, d\mathbf{x} \\ \mathcal{I}_2 := \displaystyle\int_{\mathbf{\Omega}\times\mathbb{R}} \frac{(A + r_z)^2}{2\alpha} \, \partial_t F_e \, d\mathbf{x} \, dr_z = \frac{d}{dt} \int_{\mathbf{\Omega}\times\mathbb{R}} \frac{(A + r_z)^2}{2\alpha} \, F_e \, d\mathbf{x} \, dr_z \; - \; \frac{1}{\alpha} \int_{\mathbf{\Omega}} (n_e A + \; n_e \, \mathbf{u}_e) \, \partial_t A \, d\mathbf{x}, \end{cases}$$

which yields using the equation on A in (2.15),

$$\mathcal{I}_1 + \mathcal{I}_2 = \frac{d}{dt} \int_{\mathbf{\Omega}\times\mathbb{R}} \left[\frac{(A - r_z)^2}{2} \, F_i \; + \; \frac{(A + r_z)^2}{2\alpha} \, F_e \right] d\mathbf{x} \, dr_z \; + \; \frac{1}{2 \, \mathrm{Ma}^2} \frac{d}{dt} \int_{\mathbf{\Omega}} |\nabla_{\mathbf{x}} A|^2 d\mathbf{x}.$$

On the other hand, from the equation on Φ in (2.15), we get

$$\mathcal{I}_3 := \int_{\mathbf{\Omega}\times\mathbb{R}} \partial_t (n_i - n_e) \, \Phi \, d\mathbf{x} = \frac{1}{2} \frac{d}{dt} \int_{\mathbf{\Omega}} |\nabla_{\mathbf{x}} \Phi|^2 d\mathbf{x}.$$

Finally, using that $\mathcal{I}_1 + \mathcal{I}_2 + \mathcal{I}_3 = 0$ in (2.37), we obtain the energy conservation (2.35). □

From the conservation of moments (Proposition 2.6), we get L^p estimates [5] on the macroscopic quantities

Lemma 2.7. If $F \in L^1 \cap L^\infty(\Omega \times \mathbb{R})$ and $|r_z|^m F \in L^1(\Omega \times \mathbb{R})$ with $0 \leq m < \infty$, then we define

$$n_F = \int_{\mathbb{R}} F dr_z, \quad n\mathbf{u}_F = \int_{\mathbb{R}} F\, r_z\, dr_z, \quad e_F = \int_{\mathbb{R}} F\, |r_z|^2\, dr_z$$

and there exists $C > 0$ such that

$$\|n_F\|_{L^{1+m}} \leq C\, \|F\|_{L^\infty}^{m/(m+1)} \left(\int_{\Omega\times\mathbb{R}} |r_z|^m\, |F| dr_z\, d\mathbf{x} \right)^{1/(m+1)}$$

and

$$\begin{cases} \|n\mathbf{u}_F\|_{L^{(1+m)/2}} \leq C\, \|F\|_{L^\infty}^{(m-1)/(m+1)} \left(\int_{\Omega\times\mathbb{R}} |r_z|^m\, |F| dr_z\, d\mathbf{x} \right)^{2/(m+1)}, \\ \\ \|e_F\|_{L^{(1+m)/3}} \leq C\, \|F\|_{L^\infty}^{(m-2)/(m+1)} \left(\int_{\Omega\times\mathbb{R}} |r_z|^m\, |F| dr_z\, d\mathbf{x} \right)^{3/(m+1)}. \end{cases}$$

From Proposition 2.6 and Lemma 2.7 we can prove the existence of weak solutions to (2.15)

Theorem 2.8 (Existence of weak solutions)**.** *Assume that the nonnegative initial condition $F_{s,\mathrm{in}} \in L^1 \cap L^\infty(\Omega \times \mathbb{R})$ for $s = i$, e and for any $m > 5$*

$$\int_{\Omega\times\mathbb{R}} |r_z|^m F_s(0, \mathbf{x}, r_z) dr_z\, d\mathbf{x} < \infty. \tag{2.38}$$

Then, there exists a weak solution (F_i, F_e, Φ, A) to (2.15), with F_i, $F_e \in L^\infty(\mathbb{R}^+, L^1 \cap L^\infty(\Omega \times \mathbb{R}))$, and Φ, $A \in L^\infty(\mathbb{R}^+, W_0^{1,p}(\Omega))$, for any $p > 1$.

Proof. The proof follows the lines of the existence of weak solutions for the Vlasov-Poisson system [2, 13]. The main point here is to get enough compactness on the potential A since its equation is nonlinear

$$-\Delta_{\mathbf{x}} A + \mathrm{Ma}^2 \left(n_i + \frac{n_e}{\alpha} \right) A = \mathrm{Ma}^2 \mathcal{J}_z.$$

From (2.38) and Proposition 2.6, we first get the conservation of moments for any $l \in (0, m]$ and $s = i$, e

$$\int_{\Omega\times\mathbb{R}} |r_z|^l\, F_s(t) dr_z\, d\mathbf{x} = \int_{\Omega\times\mathbb{R}} |r_z|^l\, F_{s,\mathrm{in}} dr_z\, d\mathbf{x} < \infty,$$

hence applying Lemma 2.7, it yields that for any $r \in [1, m+1]$ and $q \in [1, (m+1)/2]$

$$\rho = n_i - n_e \in L^\infty(\mathbb{R}^+, L^r(\Omega)), \quad \mathcal{J}_z \in L^\infty(\mathbb{R}^+, L^q(\Omega)).$$

Thus, from the elliptic equations in (2.15) for A and Φ,

$$\begin{cases} -\Delta_{\mathbf{x}} \Phi = \rho, \\ \\ -\Delta_{\mathbf{x}} A + \mathrm{Ma}^2 \left(n_i + \dfrac{n_e}{\alpha} \right) A = \mathrm{Ma}^2 \mathcal{J}_z, \end{cases}$$

it yields

$$\nabla_{\mathbf{x}} \Phi \in L^\infty(\mathbb{R}^+, W_0^{1,r}(\Omega)), \quad \nabla_{\mathbf{x}} A \in L^\infty(\mathbb{R}^+, W_0^{1,q}(\Omega)).$$

Since we can choose r and $q > 2$, using classical Sobolev inequalities, we have in particular that both $\nabla_{\mathbf{x}} \Phi$ and $\nabla_{\mathbf{x}} A$ are uniformly bounded in $L^\infty(\mathbb{R}^+ \times \Omega)$.

Furthermore, we obtain an estimate on the time derivative $\partial_t \nabla_{\mathbf{x}} \Phi$ and $\partial_t \nabla_{\mathbf{x}} A$ by differentiating with respect to the two Poisson equations in (2.15)

$$\begin{cases} -\Delta_{\mathbf{x}} \partial_t \Phi = \partial_t \rho, \\ \\ -\Delta_{\mathbf{x}} \partial_t A + \mathrm{Ma}^2 \left(n_i + \dfrac{n_e}{\alpha} \right) \partial_t A = \mathrm{Ma}^2\, \partial_t \mathcal{J}_z - \mathrm{Ma}^2 \left(\partial_t n_i + \dfrac{\partial_t n_e}{\alpha} \right) A. \end{cases}$$

Then using the evolution equation satisfied by ρ and $\mathcal{J}_z$

$$\begin{cases} \partial_t \rho = \nabla_{\mathbf{x}} \cdot \left(\rho \, \nabla_{\mathbf{x}}^{\perp} \Phi \; + \; \left(n_i + \dfrac{n_e}{\alpha} \right) \dfrac{\nabla_{\mathbf{x}}^{\perp} A^2}{2} \; - \; \nabla_{\mathbf{x}}^{\perp} A \, \mathcal{J}_z \right), \\ \partial_t \mathcal{J}_z = \nabla_{\mathbf{x}} \cdot \left(\mathcal{J}_z \, \nabla_{\mathbf{x}}^{\perp} \Phi \; + \; \left(n_i \mathbf{u}_i + \dfrac{n_e \mathbf{u}_e}{\alpha^2} \right) \dfrac{\nabla_{\mathbf{x}}^{\perp} A^2}{2} \; - \; \nabla_{\mathbf{x}}^{\perp} A \left(e_i - \dfrac{e_e}{\alpha^2} \right) \right), \end{cases}$$

where e_s corresponds to the second order moment in r_z,

$$e_s(t, \mathbf{x}) \; = \; \int_{\mathbb{R}} F_s(t) \, |r_z|^2 \, dr_z, \quad \text{for } s = i, \, e$$

and applying Lemma 2.7, we have that e_i, $e_e \in L^{\infty}(\mathbb{R}^+, L^2(\Omega))$, hence both terms $\partial_t \nabla_{\mathbf{x}} A$ and $\partial_t \nabla_{\mathbf{x}} \Phi$ are uniformly bounded $L^{\infty}(\mathbb{R}^+, L^2(\Omega))$.

From these estimates, we get strong compactness on the electromagnetic field $\mathbf{E} = -\nabla_{\mathbf{x}} \Phi$ and $\mathbf{B} = \nabla_{\mathbf{x}} \times A$ in L^2 and weak compactness in L^2 allowing to treat the nonlinear terms and prove existence of weak solutions for (2.15). □

Remark 2.9. Observing that starting from (2.15), and taking the limit $\mathrm{Ma} \to 0$, it gives from the Poisson's equation that $A = 0$. Then we integrate (2.15) in $r_z \in \mathbb{R}$ and we recover the two dimensional guiding-center model [21, 36, 29]

$$\begin{cases} \partial_t \rho + \nabla_{\mathbf{x}} \cdot (\mathbf{U} \, \rho) = 0, \\ \\ -\Delta_{\mathbf{x}} \Phi = \rho, \end{cases} \tag{2.39}$$

with the divergence free velocity $\mathbf{U} = -\nabla_{\mathbf{x}}^{\perp} \Phi$.

2.4. **Guiding center model & linear instability.** To study the growth rate of the linear instability for our asymptotic model (2.15), we follow the classical linearization procedure: consider an equilibrium solution $(F_{i,0}, F_{e,0}, \Phi_0, A_0)$ to (2.15) and assume that

$$\int_{\mathbb{R}} r_z \, F_{i,0} \, dr_z \; = \; \int_{\mathbb{R}} r_z \, F_{e,0} \, dr_z \; = \; 0. \tag{2.40}$$

Therefore the potential A_0 satisfies a linear Poisson equation with a null source term together with periodic boundary condition or zero Dirichlet boundary conditions, which means that $A_0 \equiv 0$.

Now we consider (F_i, F_e, Φ, A) a solution to the nonlinear system ((2.15)) and decompose it as the sum of the equilibrium $(F_{i,0}, F_{e,0}, \Phi_0, 0)$ and a perturbation (F_i', F_e', Φ', A') ,

$$F_i = F_{i,0} + F_i', \;\; F_e = F_{e,0} + F_e', \;\; \rho = \rho_0 + \rho', \;\; \Phi = \Phi_0 + \Phi', \;\; A = A'.$$

Then we substitute them into (2.15) and drop the high order small perturbation terms, a linearized system is obtained as follows:

$$\begin{cases} \partial_t F_i' \; - \; \nabla_{\mathbf{x}}^{\perp} \Phi_0 \cdot \nabla_{\mathbf{x}} F_i' - \nabla_{\mathbf{x}}^{\perp} \left(\Phi' - p_z A' \right) \cdot \nabla_{\mathbf{x}} F_{i,0} \; = \; 0, \\ \\ \partial_t F_e' \; - \; \nabla_{\mathbf{x}}^{\perp} \Phi_0 \cdot \nabla_{\mathbf{x}} F_e' - \nabla_{\mathbf{x}}^{\perp} \left(\Phi' - \dfrac{q_z}{\alpha} A' \right) \cdot \nabla_{\mathbf{x}} F_{e,0} \; = \; 0, \\ \\ -\Delta_{\mathbf{x}} \Phi' \; = \; \rho', \\ \\ -\Delta_{\mathbf{x}} A' \; + \; \mathrm{Ma}^2 \left(n_{i,0} + \dfrac{n_{e,0}}{\alpha} \right) A' \; = \; \mathrm{Ma}^2 \, \mathcal{J}_z' := \mathrm{Ma}^2 \displaystyle\int_{\mathbb{R}} r_z \left(F_i' - \frac{F_e'}{\alpha} \right) dr_z. \end{cases} \tag{2.41}$$

Now we integrate the first equation in $p_z \in \mathbb{R}$ and the second one in $q_z \in \mathbb{R}$ and using (2.40), we get a linearized system for the perturbed charge density

$$\begin{cases} \partial_t \rho' \; - \; \nabla_{\mathbf{x}}^{\perp} \Phi_0 \cdot \nabla_{\mathbf{x}} \rho' - \nabla_{\mathbf{x}}^{\perp} \Phi' \cdot \nabla_{\mathbf{x}} \rho_0 \; = \; 0, \\ \\ -\Delta_{\mathbf{x}} \Phi' \; = \; \rho', \end{cases} \tag{2.42}$$

which is exactly the linearized system for the two dimensional guiding-center model (2.39).

Therefore, from an equilibrium (ρ_0, Φ_0) for the guiding-center model (2.39), we can easily construct an equilibrium for (2.15) by choosing $F_{s,0}$ such that it satisfies (2.40) and

$$\int_{\mathbb{R}} F_{s,0}\, dr_z \;=\; n_{s,0}, \quad \text{for } s = i,\, e. \tag{2.43}$$

where $n_{s,0}$ is the equilibrium density satisfying $\rho_0 = n_{i,0} - n_{e,0}$. For instance, we can choose

$$F_{s,0} = \frac{n_{s,0}}{\sqrt{2\pi}} \exp\left(-\frac{r_z^2}{2}\right).$$

In terms of the electric charge density ρ and potential Φ, our asymptotic model has the same mechanism for generating instabilities as the two dimensional guiding-center model, so that the growth rate of instabilities for the electric field will be the same. We can refer to [33, 29, 11] for the analytical and numerical studies of the two dimensional guiding-center model. In the next section, we will numerically verify that the linear growth rates of instabilities for the electric potential of the two models are the same.

From this point, we observe that by choosing a nonzero initial potential A, that is a small current density $\mathcal{J}_z$, we can initiate an instability on the asymptotic model (2.15), whereas the purely electrostatic guiding center model remains stationary.

Remark 2.10. We would notice that for the distribution function F_i or F_e, due to the extra term of $\nabla_{\mathbf{x}}^{\perp}(p_z A') \cdot \nabla_{\mathbf{x}} F_{i,0}$ and $\nabla_{\mathbf{x}}^{\perp}(q_z A'/\alpha) \cdot \nabla_{\mathbf{x}} F_{e,0}$ in the first two equations of (2.41), some other instabilities might also happen to F_i' or F_e', which is much more complicated to analyze.

3. Numerical scheme

In this section, we will describe a high order numerical scheme for solving the asymptotic kinetic model (2.15), which depends on $(\mathbf{x}, p_z)$ or $(\mathbf{x}, q_z)$ and time t. We will apply a conservative finite difference scheme with Hermite weighted essentially non-oscillatory (WENO) reconstruction for solving the conservative transport equations. The Poisson's equation for the electric potential function Φ will be solved by a 5-point central finite difference discretization for Dirichlet boundary conditions, or by the fast Fourier transform (FFT) for periodic boundary conditions on a rectangular domain. The elliptic equation for the magnetic potential A is solved by a 5-point central finite difference discretization. The methods described here are natural extensions of those proposed in [36] for solving the two dimensional guiding-center model (2.39), which we will also adopt here for comparison in the numerical tests. In the following, we will briefly review these methods and explicitly mention the main differences, we refer to [36] for more details. Besides, since some instability problems and the linear growth rates will be numerically studied in the next section, at the end of this section, we will linearize the asymptotic kinetic model (2.15) and build a link to the two dimensional guiding-center model (2.39) as is analyzed in [33].

3.1. Hermite WENO finite difference scheme for the transport equation.

We consider the transport equation for ions in a conservative form

$$\partial_t F_i + \nabla_{\mathbf{x}} \cdot (\mathbf{U}_i F_i) = 0,$$

with $F_i = F_i(t, \mathbf{x}, p_z)$ and $\mathbf{U}_i = \mathbf{U}_i(t, \mathbf{x}, p_z)$, first in the moment p_z direction we consider a cut-off domain of $\Omega_c = [-V_c, V_c]$, where V_c is large enough so that F_i outside it is nearly zero. We take a uniform discretization with N_c grid points on Ω_c. Since p_z in F_i is a dummy argument, on each fixed p_z the transport equation can be taken as a $2d$ problem on $\mathbf{x}$. A finite difference scheme for the two dimensional transport equation is applied dimension by dimension, similarly for the transport equation of the electrons. In the following we will only need to describe a Hermite WENO reconstruction for a $1d$ transport equation.

Let us consider a prototype $1d$ conservative transport equation

$$f_t + (uf)_x = 0, \tag{3.1}$$

with velocity $u = u(t,x)$. We assume a uniform discretization of the computational domain $[x_{min}, x_{max}]$ with N_x grid points

$$x_{min} = x_0 < x_1 < \cdots < x_{N_x-2} < x_{N_x-1} = x_{max},$$

where the mesh size is $\Delta x = x_{k+1} - x_k$ for $0 \le k < N_x$. A conservative finite difference scheme for (3.1) can be written as

$$f_i^{n+1} = f_i^n - \frac{\Delta t}{\Delta x}\left(\hat{h}_{i+\frac{1}{2}} - \hat{h}_{i-\frac{1}{2}}\right),$$

where $\Delta t = t^{n+1} - t^n$ and f_i^n is the numerical point value at time level t^n on the grid point x_i. $\hat{h}_{i+\frac{1}{2}}$ is an upwind numerical flux, which is defined as

$$\hat{h}_{i+\frac{1}{2}} = \begin{cases} h^-_{i+\frac{1}{2}}, & \text{if } \frac{u_i^n + u_{i+1}^n}{2} > 0, \\ h^+_{i+\frac{1}{2}}, & \text{otherwise .} \end{cases}$$

$h^{\pm}_{i+\frac{1}{2}}$ are the fluxes reconstructed from $\{h_i^n = u_i^n f_i^n\}_i$ by a Hermite WENO reconstruction, from the left and right sides of $x_{i+\frac{1}{2}}$ respectively. u_i^n is the numerical velocity approximating $u(t^n, x_i)$.

In this paper, we adopt a fifth order Hermite WENO reconstruction to compute $h^-_{i+\frac{1}{2}}$. The procedure is outlined as follows. $h^+_{i+\frac{1}{2}}$ can be obtained in mirror symmetric with respect to $x_{i+\frac{1}{2}}$. For simplicity, we drop the superscript n for h_i^n and we have

$$h^-_{i+\frac{1}{2}} = \omega_l h_l(x_{i+\frac{1}{2}}) + \omega_c h_c(x_{i+\frac{1}{2}}) + \omega_r h_r(x_{i+\frac{1}{2}}).$$

The three polynomials $h_l(x)$, $h_c(x)$ and $h_r(x)$ evaluating at $x_{i+\frac{1}{2}}$ are

$$h_l(x_{i+\frac{1}{2}}) = -2h_{i-1} + 2h_i + G'_{i-\frac{3}{2}}, \quad h_c(x_{i+\frac{1}{2}}) = \frac{-h_{i-1} + 5h_i + 2h_{i+1}}{6}, \quad h_r(x_{i+\frac{1}{2}}) = \frac{h_i + 5h_{i+1} - 2G'_{i+\frac{3}{2}}}{4}.$$

The derivative of the primitive function $G'_{i+\frac{1}{2}}$ is given by a 6th order central difference approximation

$$G'_{i+\frac{1}{2}} = \frac{1}{60}\big[(h_{i+3} - h_{i-2}) - 8(h_{i+2} - h_{i-1}) + 37(h_{i+1} - h_i)\big].$$

ω_l, ω_c and ω_r are the nonlinear WENO weights and determined according to the smoothness indicators

$$\omega_k = \frac{\alpha_k}{\alpha_l + \alpha_c + \alpha_r}, \quad \alpha_k = \frac{c_k}{(\epsilon + \beta_k)^2}, \quad k = l, c, r.$$

The linear coefficients are $c_l = 1/9$ and $c_c = c_r = 4/9$, and the small parameter $\epsilon = 10^{-6}$ is to avoid the denominator to be 0.

To evaluate the smooth indicators β_l, β_c and β_r, we would note that here we measure them on the cell $[x_{i-\frac{1}{2}}, x_{i+\frac{1}{2}}]$ instead of $[x_i, x_{i+1}]$ as in [36]. In this way, the smooth indicators are symmetric with respect to x_i, as we can see below:

$$\begin{aligned}
\beta_l &= \int_{x_{i-\frac{1}{2}}}^{x_{i+\frac{1}{2}}} \Delta x (h_l'(x))^2 + \Delta x^3 (h_l''(x))^2 dx \\
&= \frac{13}{16}s_1^2 + \frac{3}{16}(s_1 - 4s_2)^2, \text{ with } s_1 = h_{i-1} - h_i, \quad s_2 = -3h_{i-1} + h_0 + G'_{i-\frac{3}{2}}, \\
\beta_c &= \int_{x_{i-\frac{1}{2}}}^{x_{i+\frac{1}{2}}} \Delta x (h_c'(x))^2 + \Delta x^3 (h_c''(x))^2 dx \\
&= \frac{1}{4}s_1^2 + \frac{13}{12}s_2^2, \text{ with } s_1 = h_{i+1} - h_{i-1}, \quad s_2 = h_{i+1} - 2h_0 + h_{i-1}, \\
\beta_r &= \int_{x_{i-\frac{1}{2}}}^{x_{i+\frac{1}{2}}} \Delta x (h_r'(x))^2 + \Delta x^3 (h_r''(x))^2 dx \\
&= \frac{13}{16}s_1^2 + \frac{3}{16}(s_1 - 4s_2)^2, \text{ with } s_1 = h_{i+1} - h_i, \quad s_2 = -3h_{i+1} + h_0 + G'_{i+\frac{3}{2}}.
\end{aligned}$$

Remark 3.1. For the two dimensional transport equation with Dirichlet boundary conditions, and/or if the physical domain is not rectangular, e.g. a disk, an inverse Lax-Wendroff method [17] can be used to deal with the curved boundary conditions inside a larger rectangular computational domain.

3.2. **Discretization of the elliptic equations.** There are two elliptic equations in (2.15): one is the Poisson's equation for the electric potential Φ, the other is the Poisson's equation with another quasilinear term $\mathrm{Ma}^2\left(n_i+\frac{n_e}{\alpha}\right)A$ for the magnetic potential A. For the Poisson's equation of the electric potential Φ, if it is defined on a rectangular domain with periodic boundary conditions, it can be easily solved by FFT. Otherwise, a classic 5-point central finite difference approximation is used to discretize the Laplacian operator. For the elliptic equation of the magnetic potential A, since the quasilinear term has the coefficient $\mathrm{Ma}^2\left(n_i+\frac{n_e}{\alpha}\right)A$ which depends on $\mathbf{x}$, FFT is not available, we will always use the 5-point central finite difference approximation. We notice that $\mathrm{Ma}^2\left(n_i+\frac{n_e}{\alpha}\right)$ is always positive to ensure a positive definite mass matrix. Here the density n_s defined in (2.16) and current density $\mathcal{J}_z$ in (2.17), are integrated by a mid-point rule with spectral accuracy [6].

For a problem with curved physical boundary, e.g., a disk, some points of the 5-point discretization of the Laplacian operator near the boundary might not always be available. The method developed for the two dimensional guiding-center model in [36] can be used here. The main idea is that if a grid point $\mathbf{x}_g$ is outside of the interior domain, it is extrapolated by some interior points $\mathbf{x}_h$ and $\mathbf{x}_{2h}$ along the normal direction going through $\mathbf{x}_g$ (see Fig. 6 in [36]). These interior points are selected with equal distance $h=\min(\Delta x,\Delta y)$, starting from the cross point of the normal vector and the physical boundary at $\mathbf{x}_p$, that is $h=|\mathbf{x}_p-\mathbf{x}_h|=|\mathbf{x}_h-\mathbf{x}_{2h}|$. Then the interior points $\mathbf{x}_h$ and $\mathbf{x}_{2h}$ are interpolated by a Lagrangian polynomial reconstructed from 9 nearest points, which are adjacent to the cross points of the normal vector with the grid lines around $\mathbf{x}_h$ and $\mathbf{x}_{2h}$. For some wild geometries, if 9 points are not all available, we turn to use lower order Lagrangian polynomials with four points or even one point.

4. Numerical Examples

In this section, several numerical tests are performed to illustrate the properties of the the asymptotic kinetic model (2.15) involving a self-consistent electromagnetic field and to compare the results with those obtained with the macroscopic guiding-center model (2.39) taking into account only electrostatic effects [36, 29]. The scheme described in the above section coupled with a fourth-order Runge-Kutta scheme for the time discretization is adopted. Three examples are considered: a linear equation with prescribed electromagnetic field, the diocotron instability problem and the Kelvin-Helmholtz instability problem. We mainly show that the new asymptotic model (2.15) can generate the same instability as the two dimensional guiding-center model (2.39), while some other instabilities can also be created due to some small perturbations purely in the self-consistent magnetic field.

In the following, for the asymptotic kinetic model (2.15), we all take the cut-off domain in velocity as $[-8,8]$ and discretize it with $N=32$ uniform grid points.

4.1. **Linear equation.** In the first example, we consider a problem with a given electromagnetic field $\mathbf{E}\equiv-\nabla_{\mathbf{x}}\Phi(\mathbf{x})$ and $\mathbf{B}=\nabla_{\mathbf{x}}\times A(\mathbf{x})$, hence we set the Hamiltonian

$$\mathcal{H}=\Phi+\frac{1}{2}\left(A-p_z\right)^2$$

and the distribution function $F\equiv F(t,\mathbf{x},p_z)$ is a solution to

$$\partial_t F-\nabla_{\mathbf{x}}^{\perp}\mathcal{H}\cdot\nabla_{\mathbf{x}}F=0, \tag{4.1}$$

which is supplemented by an initial data F_0 and periodic boundary conditions in $\mathbf{x}$. Moreover, both potentials Φ and A are prescribed so that the velocity field is given and does not depend on time.

The initial distribution function F is chosen as

$$F_0(\mathbf{x},p_z)=\frac{n_0(\mathbf{x})}{\sqrt{2\pi}}\exp\left(-\frac{(p_z-u_0(\mathbf{x}))^2}{2}\right), \tag{4.2}$$

with $n_0(\mathbf{x}) = \sin(y)$ set on a square $[0, 4\pi] \times [0, 2\pi]$ and a shift $u_0(\mathbf{x})$ in the p_z direction as

$$u_0(\mathbf{x}) = -\cos\left(\frac{x}{2}\right). \tag{4.3}$$

Furthermore the magnetic potential is chosen to be $A = -0.05\sin(x/2)$, which induces a drift in the y direction, whereas the electric potential is $\Phi = \sin(y)$, which generates a drift in the x direction.

Observe that with such a choice, (n_0, Φ) is an exact solution to the stationary linear guiding center model

$$-\nabla_{\mathbf{x}}^{\perp}\Phi \cdot \nabla_{\mathbf{x}} n = 0, \tag{4.4}$$

but not to the linear kinetic model (4.1) due to the drift u_0 and the magnetic potential A.

This numerical test illustrates that even a small magnetic potential A may generate a drift and oscillations in space which cannot be observed on the purely electrostatic case when we neglect the magnetic field generated by the potential A.

On the one hand, we present in Figure 4.1 the numerical results corresponding to (4.1) with a grid $N_x \times N_y = 256 \times 256$. Due to the effect of the drift from the magnetic field A, we can observe highly oscillatory solutions in the y direction on the density n given by

$$n(t, \mathbf{x}) \;=\; \int_{\mathbb{R}} F(t, \mathbf{x}, p_z) dp_z.$$

It is worth to mention here that no oscillation occurs when the magnetic potential A is set to be zero.

We also observe that since Φ and A do not depend on time, the total energy defined in (2.35) corresponding to the Hamiltonian $\mathcal{H}$, is still conserved with respect to time and all L^p norms are also conserved. In Figure 4.2, we show the time evolution of the relative error for the total energy (2.35), the L^2 norm of F. For this linear problem, these quantities are preserved well and the minimum bound of F is also strictly maintained.

4.2. **Diocotron instability.** We set

$$\mathcal{H} = \Phi + \frac{1}{2}(A - p_z)^2$$

and consider the nonlinear asymptotic model (2.15) where the density of electrons is neglected and the reduced distribution function of ions is denoted by F and is a solution to

$$\begin{cases} \partial_t F - \nabla_{\mathbf{x}}^{\perp}\mathcal{H} \cdot \nabla_{\mathbf{x}} F \;=\; 0, \\ \\ -\Delta\Phi \;=\; n, \\ \\ -\Delta A \,+\, \mathrm{Ma}^2\, n\, A \;=\; \mathrm{Ma}^2\, \mathcal{J}_z, \end{cases} \tag{4.5}$$

where

$$n \;=\; \int_{\mathbb{R}} F(t)\, dp_z, \quad \mathcal{J}_z \;=\; \int_{\mathbb{R}} F(t) p_z\, dp_z.$$

This solution can be compared to the two dimensional guiding center model (2.39), where we neglect the effect of the self-consistent magnetic field $\mathbf{B} = \nabla_{\mathbf{x}} \times A$, corresponding to the low Mach number limit $\mathrm{Ma} \to 0$ of (4.5), it yields

$$\begin{cases} \partial_t n - \nabla_{\mathbf{x}}^{\perp}\Phi \cdot \nabla_{\mathbf{x}} n \;=\; 0, \\ \\ -\Delta\Phi = n. \end{cases} \tag{4.6}$$

In this example, we choose $\mathrm{Ma} = 0.1$ and we would like to verify that the asymptotic kinetic model (4.5) has indeed the same instability on the density n as compared to the two dimensional guiding-center model (4.6). We choose a discontinuous initial density n_0 which is linearly unstable [11, 29].

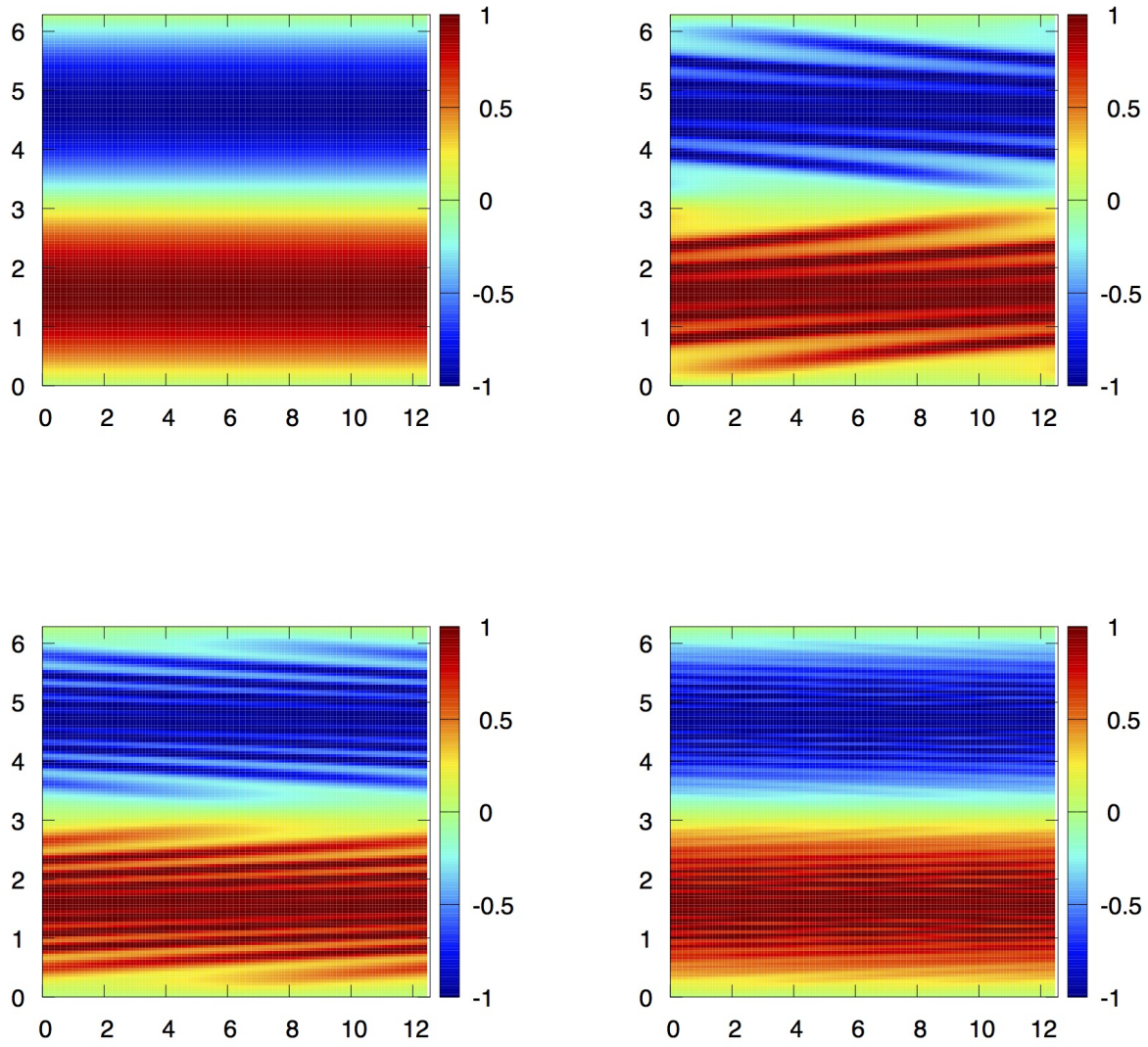

FIGURE 4.1. **Linear equation.** The density n with a given electromagnetic field for the $2d \times 1d$ asymptotic model (2.15). From left to right, top to bottom: $t = 40, 60, 80, 100$.

Therefore, we consider Ω as a ball centered in 0 of radius $R = 10$ with the initial density

$$n_0(\mathbf{x}) = \begin{cases} 1 + \varepsilon \cos(l\theta), & \text{if } r^- \leq \sqrt{x^2 + y^2} \leq r^+, \\ 0, & \text{else,} \end{cases} \tag{4.7}$$

where $\varepsilon = 0.02$, $l = 3$, $r^- = 3$, $r^+ = 5$, which will create a small instability for the two-dimensional model (4.6).

Now for the asymptotic model (4.5), we still consider the same density n_0 as an initial data, but introduce an additional perturbation on the moment p_z by choosing

$$F_0(\mathbf{x}, p_z) = \frac{n_0(\mathbf{x})}{\sqrt{2\pi}} \exp\left(-\frac{(\, p_z - u_0(\mathbf{x})\,)^2}{2} \right). \tag{4.8}$$

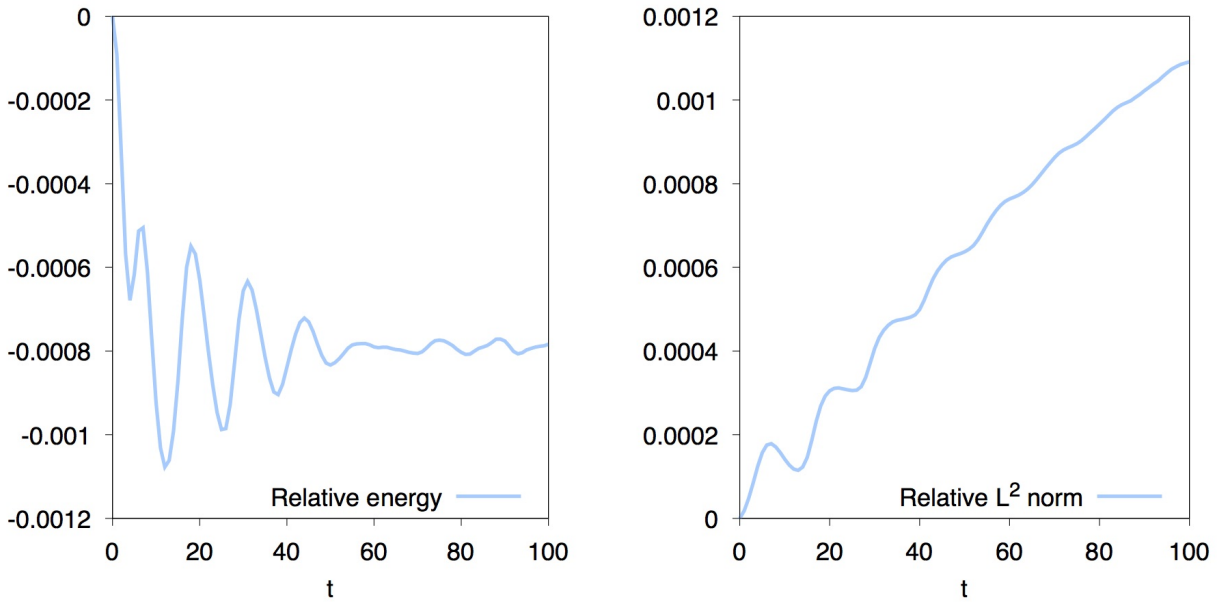

(a) (b)

FIGURE 4.2. **Linear equation.** Time evolution of the relative error of the total energy (2.35), the L^2 norm of F for the $2d \times 1d$ asymptotic model (2.15).

with $u_0 = \delta \cos(m\,\theta)$, where $\theta = \text{atan2}(y, x)$, $\delta = 0.1$, $m = 3$. It is expected that the instability will now be driven by the perturbation on the density n_0 corresponding to the mode $l = 3$ but also by the perturbation on the current density $\mathcal{J}_z$ due to u_0 corresponding to the mode $m = 3$.

In Figure 4.3, we can clearly see three vortexes are formed at $t = 40$, which is the same as the diocotron instability for the two dimensional guiding-center model (4.6) and agrees with the linear instability analysis in Section 2.4. At $t = 60, 80, 100$, these vortexes continue moving and start to mix with each other. Here the grid is $N_x \times N_y = 600 \times 600$. However, we would notice that for the current density $\mathcal{J}_z$, as shown in Figure 4.4, we can also observe three vortexes, which might be caused by the perturbation on the moment p_z from the self-consistent magnetic field which are different from the instabilities of the density n.

In Figure 4.5, we show the time evolution of the L^∞ norm for the difference of the electrical potential $\|\Phi(t) - \Phi(0)\|_{L^\infty}$ and $\|A(t)\|_{L^\infty}$, on the grids of $N_x \times N_y = 600 \times 600$ and $N_x \times N_y = 300 \times 300$. We can see convergent results. Especially an exponential growth rate on $\|\Phi(t) - \Phi(0)\|_{L^\infty}$ can be observed for $t < 50$, while the magnitude of the self-consistent magnetic field A is at the level of 10^{-4}. We measure the growth rate for $\|\Phi(t) - \Phi(0)\|_{L^\infty}$ by taking the time interval $[10, 30]$, so the growth rate is about 0.0999. The growth rate from a linear instability analysis based on the formula (6.38)-(6.42) in [11] with $\omega_D = 1/2$, is about 0.1051. These two growth rates agree with each other very well.

We also note that for this example, the dominating instability would be caused by the perturbation on the initial density n_0. Numerically we observe the exponential growth rate of $\|\Phi(t) - \Phi(0)\|_{L^\infty}$ for the two dimensional guiding center model is almost the same as the asymptotic model and we omit them in Figure 4.5 for clarity.

Then we show the time evolution of the relative difference for the total energy (2.35), the L^2 norm of F in Figure 4.6, on the grids of $N_x \times N_y = 600 \times 600$ and $N_x \times N_y = 300 \times 300$. These quantities are preserved relatively well and the total energy can be greatly improved by mesh refinement.

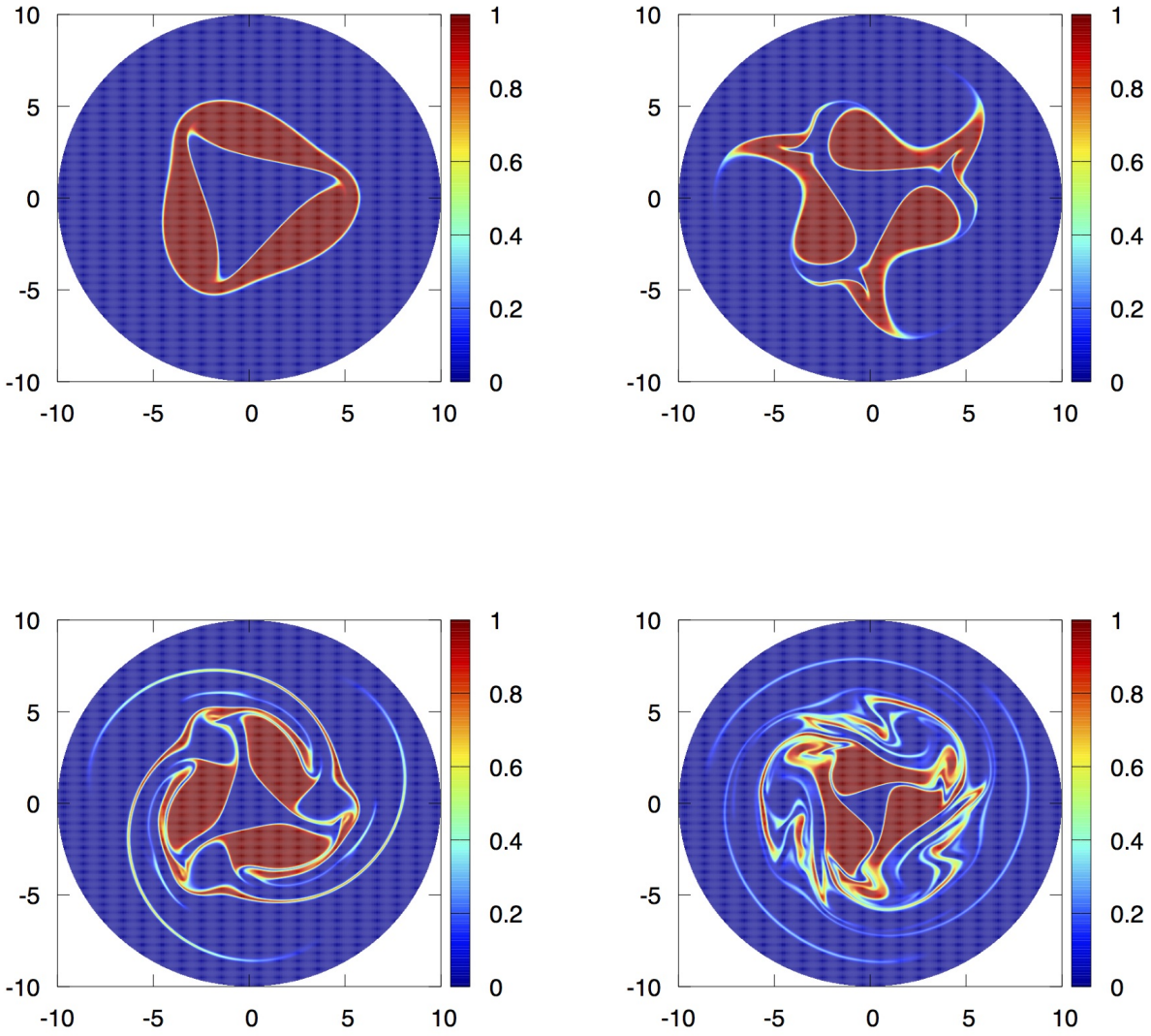

FIGURE 4.3. **Diocotron instability.** The density n for the $2d \times 1d$ asymptotic model (2.15). From left to right, top to bottom: $t = 40, 60, 80, 100$.

4.3. **Kelvin-Helmholtz instability.** In this example, we consider a plasma for ions with a neutral background. The distribution function F of the asymptotic model (4.5) for the ions is a solution to the following system

$$
\left\{
\begin{array}{l}
\partial_t F - \nabla_{\mathbf{x}}^{\perp}\left(\Phi + \dfrac{A^2}{2} - p_z A\right) \cdot \nabla_{\mathbf{x}} F \;=\; 0, \\[2ex]
-\Delta_{\mathbf{x}} \Phi = \rho \;:=\; n - n_e, \\[2ex]
-\Delta_{\mathbf{x}} A \;+\; \mathrm{Ma}^2 \left(n + \dfrac{n_e}{\alpha}\right) A = \mathrm{Ma}^2 \mathcal{J}_z,
\end{array}
\right. \tag{4.9}
$$

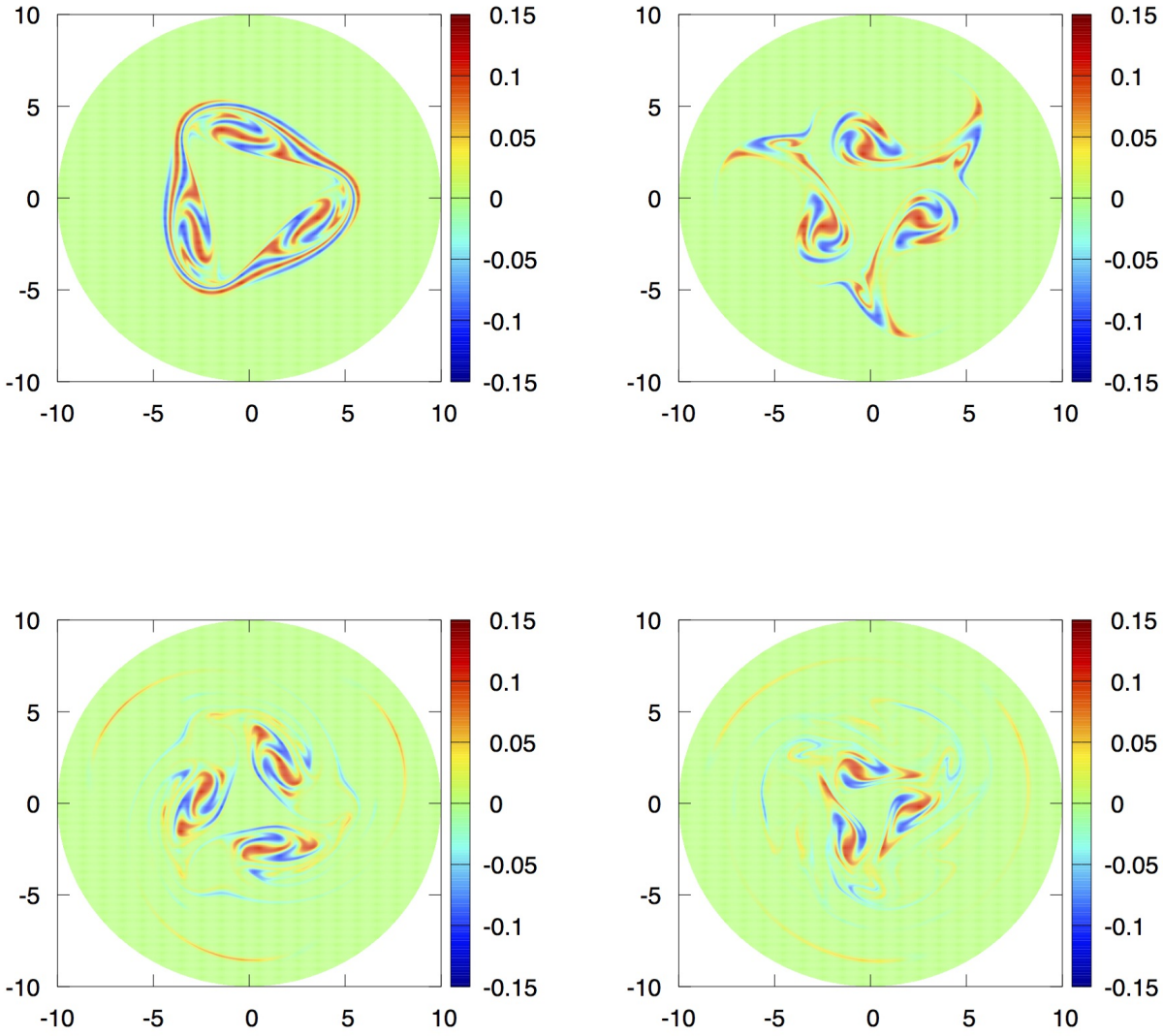

FIGURE 4.4. **Diocotron instability.** The current density $\mathcal{J}_z$ for the $2d \times 1d$ asymptotic model (2.15). From left to right, top to bottom: $t = 40, 60, 80, 100$.

with $\alpha = 1/1836.5$ which corresponds to the mass ratio of one electron and one proton. The current density is

$$\mathcal{J}_z = \int_{\mathbb{R}} F(t) p_z dp_z$$

and we choose the initial density n for the ions to be

$$n_0(\mathbf{x}) = 2 + \sin y, \tag{4.10}$$

while for the electrons, we fix it with $n_e = 2$ so that the spatial average of the total charge density $\rho = n - n_e$. We take the initial distribution function F of the ions as

$$F_0(\mathbf{x}, p_z) = \frac{n_0(\mathbf{x})}{\sqrt{2\pi}} \exp\left(-\frac{(p_z - u_0(\mathbf{x}))^2}{2}\right), \tag{4.11}$$

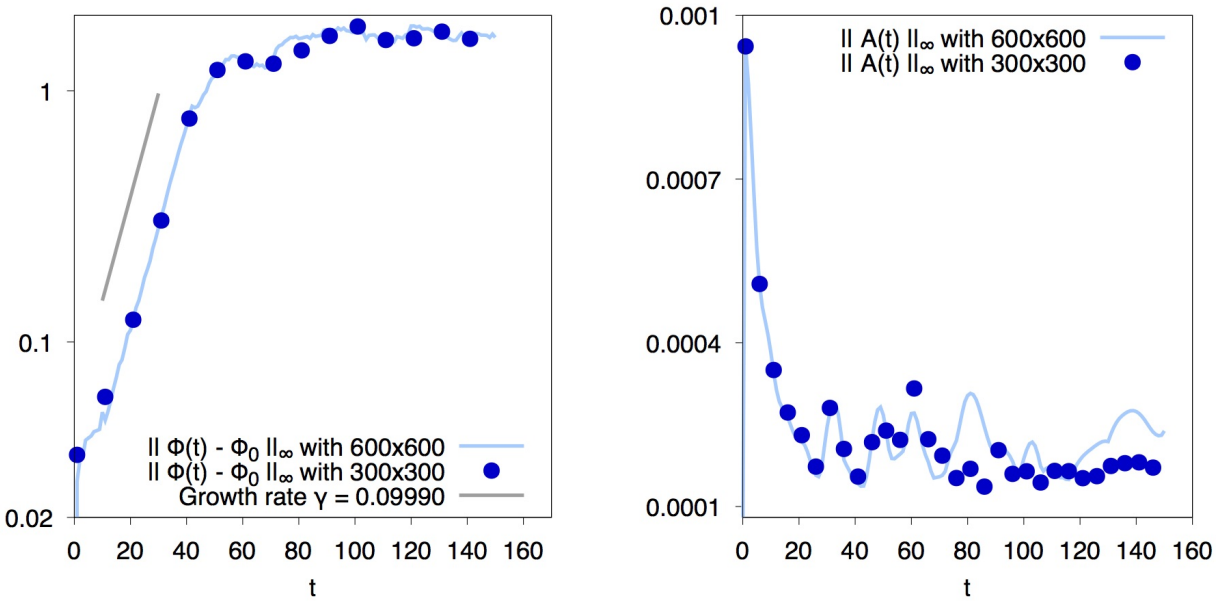

(a) (b)

FIGURE 4.5. **Diocotron instability.** Time evolution of the norm $\|\Phi(t) - \Phi(0)\|_{L^\infty}$ and $\|A(t) - A(0)\|_{L^\infty}$ for the $2d \times 1d$ asymptotic model (2.15).

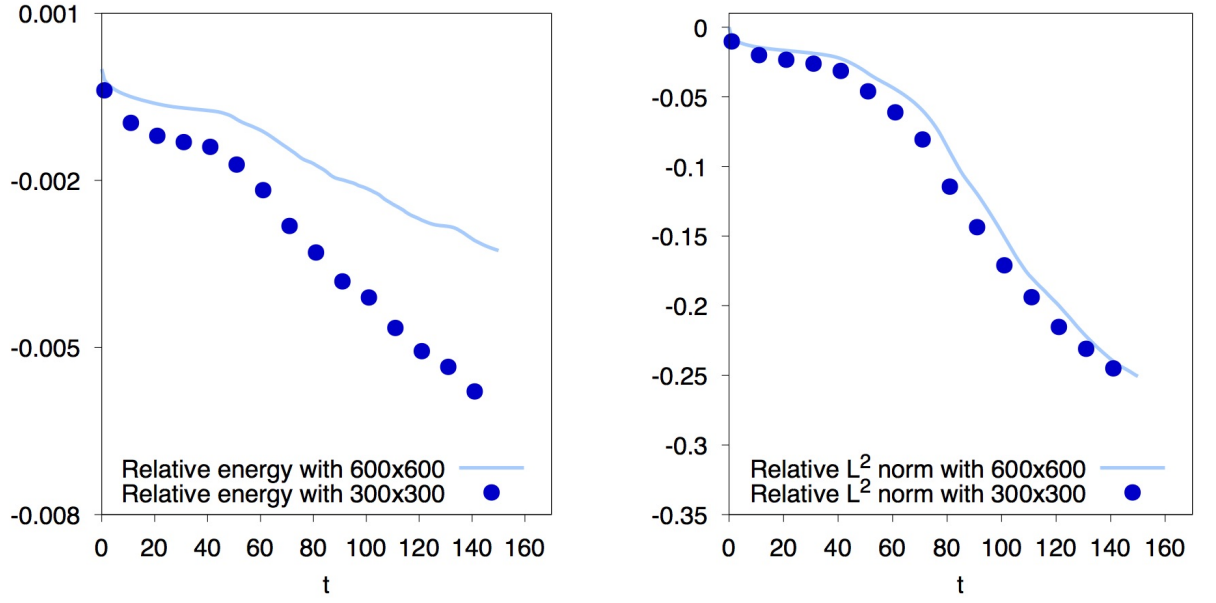

(a) (b)

FIGURE 4.6. **Diocotron instability.** Time evolution of the relative error of the total energy (2.35), the L^2 norm of F for the $2d \times 1d$ asymptotic model (2.15).

where the shifted velocity $u_0(\mathbf{x})$ is

$$u_0(\mathbf{x}) = -0.01 \left(\sin\left(\frac{x}{2}\right) - \cos(y) \right), \tag{4.12}$$

which contributes as a small perturbation in the p_z direction and its corresponding initial current density $\mathcal{J}_z$ will be small but nonzero. The distribution function of the electrons F_e is set to be at an

equilibrium as

$$F_e := F_e(q_z) = \frac{n_e}{\sqrt{2\pi}} \exp\left(-\frac{q_z^2}{2}\right),$$

so that $\int_{\mathbb{R}} F_e(r_z) r_z dr_z = 0$ and it does not contribute to the total current $\mathcal{J}_z$ in the equation of (2.17) for the magnetic potential A. Similarly if we neglect the effect of the self-consistent magnetic field $\mathbf{B}$, which corresponds to the low Mach limit $\mathrm{Ma} \to 0$ of (4.9), it yields the two-dimensional guiding center model in the following form

$$\begin{cases} \partial_t n - \nabla_{\mathbf{x}}^{\perp}\Phi \cdot \nabla_{\mathbf{x}} n = 0, \\ \\ -\Delta\Phi = n - n_e. \end{cases} \tag{4.13}$$

The computational domain is in a square $[0, 4\pi] \times [0, 2\pi]$ with periodic boundary conditions and the Mach number in (4.9) is taken to be $\mathrm{Ma} = 0.1$.

Here we see that without perturbation on the initial data (4.10), the density n of the $2d$ guiding-center model (4.13) is a the steady state $n(t, \mathbf{x}) = \sin(y)$. Furthermore, when we choose $u_0 \equiv 0$, the solution is a steady state for both models (4.13) and (4.9) and remains stable on the time interval $[0, 100]$. However, for the asymptotic model (4.9) with a non zero u_0 as (4.12), due to the effect of the self-consistent magnetic field A and a small nonzero current $\mathcal{J}_z$, we observe in Figure 4.7 that some instabilities are created on the density n at $t = 40, 60, 80, 100$. Here the grid is $N_x \times N_y = 256 \times 256$. These instabilities are very similar to the Kelvin-Helmholtz instability for the $2d$ guiding-center model (4.13) as compared to Figure 9 in [18], which do not happen on the current settings. Moreover, these instability structures can also be observed on the current density $\mathcal{J}_z$ as shown in Figure 4.8, which greatly indicate the capability of the self-consistent magnetic field as another source on the development of physical instabilities.

For the $2d \times 1d$ asymptotic model, in Figure 4.9 we show the time evolution of the L^∞ norm for the difference of the electrical potential $\|\Phi(t) - \Phi(0)\|_{L^\infty}$ and $\|A(t)\|_{L^\infty}$, on the grids of $N_x \times N_y = 256 \times 256$ and $N_x \times N_y = 128 \times 128$. The results are also convergent and an exponential growth rate is observed for $\|\Phi(t) - \Phi(0)\|_{L^\infty}$ for $t < 65$, which explicitly demonstrates the instabilities caused by the small current density $\mathcal{J}_z$ on the self-consistent magnetic field A, even we notice that the magnitude of A is overall getting smaller as shown on the right side of Figure 4.9. Here we are also able to measure the growth rate for $\|\Phi(t) - \Phi(0)\|_{L^\infty}$ by taking the time interval $[20, 40]$, the growth rate is about 0.2606, which is very close to the growth rate from the numerical predicted value 0.26 in [33] (see Figure 1 with $k_y = 0.5$ and $k_{ys} = 1$) for the two dimensional nonlinear guiding-center model, which indicates that the instability for these two models might be similar.

We show the time evolution of the relative difference for the total energy (2.35), the L^2 norm of F in Figure 4.10, on the grids of $N_x \times N_y = 256 \times 256$ and $N_x \times N_y = 128 \times 128$. These quantities are preserved well, which are similar to the last example.

5. Conclusion

In this paper, an asymptotic kinetic model is derived from a $2d \times 3d$ Vlasov-Maxwell system, by taking into account of the self-consistent magnetic field. We have assumed both a large applied magnetic field and large time in the asymptotic limit. The new asymptotic model could validate some effect on the dynamics of the plasma from the self-consistent magnetic field, even if initially the current is small, as compared to the two dimensional guiding-center model for the Vlasov-Poisson system. Numerical examples demonstrate the good properties of our new model.

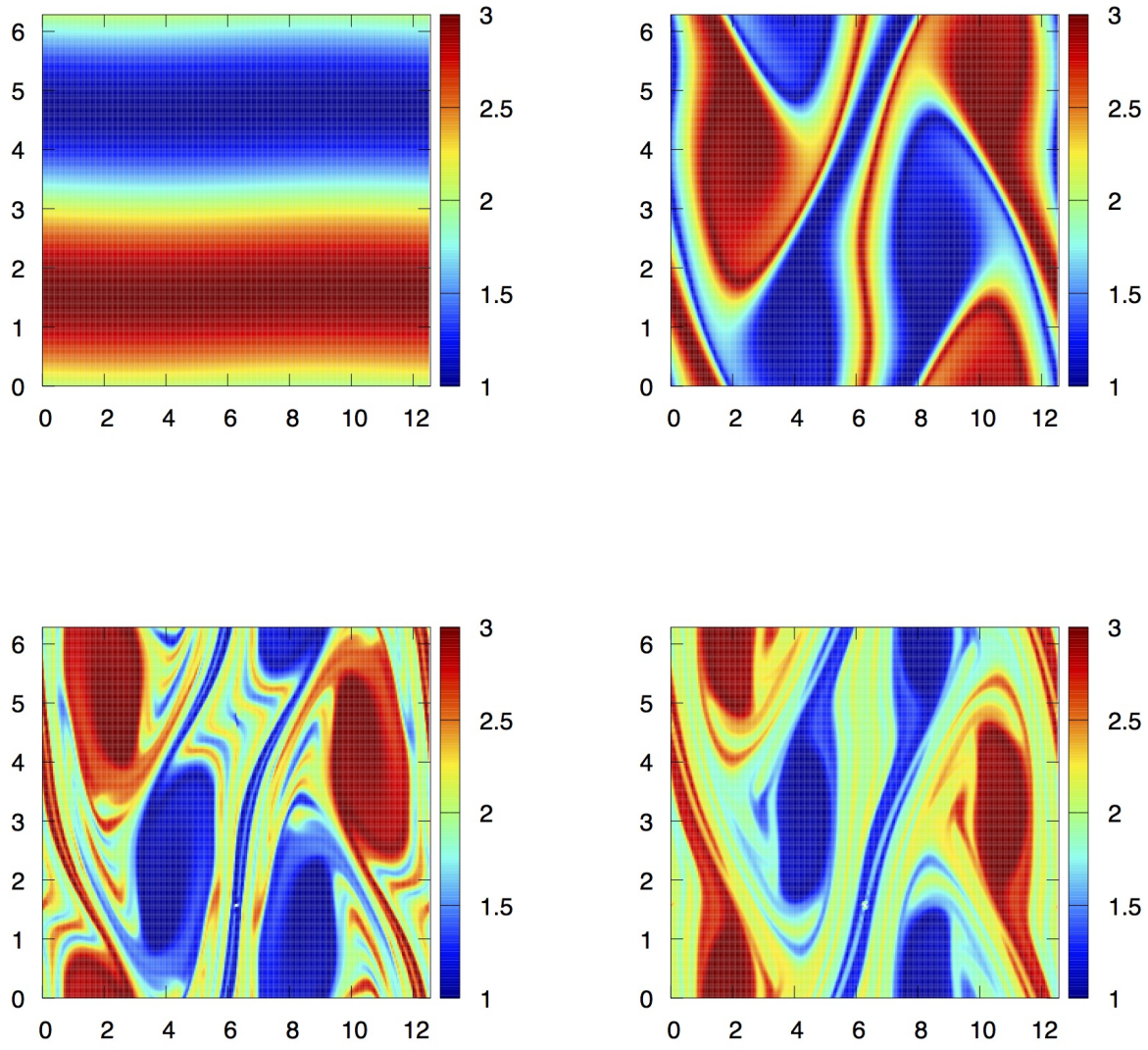

FIGURE 4.7. **Kelvin-Helmholtz instability.** The density n for the $2d \times 1d$ asymptotic model (4.9). From left to right, top to bottom: $t = 40, 60, 80, 100$.

ACKNOWLEDGEMENT

Francis Filbet and Eric Sonnendrücker were supported by the EUROfusion Consortium and has received funding from the Euratom research and training programme 2014-2018 under grant agreement No 633053. The views and opinions expressed herein do not necessarily reflect those of the European Commission.

T. Xiong acknowledges support from the Marie Skłodowska-Curie Individual Fellowships H2020-MSCA-IF-2014 of the European Commision, under the project HNSKMAP 654175. This work has also been supported by the Fundamental Research Funds for the Central Universities No. 20720160009 and National Natural Science Foundation of China (NSFC) under grants 11601455, U1630247.

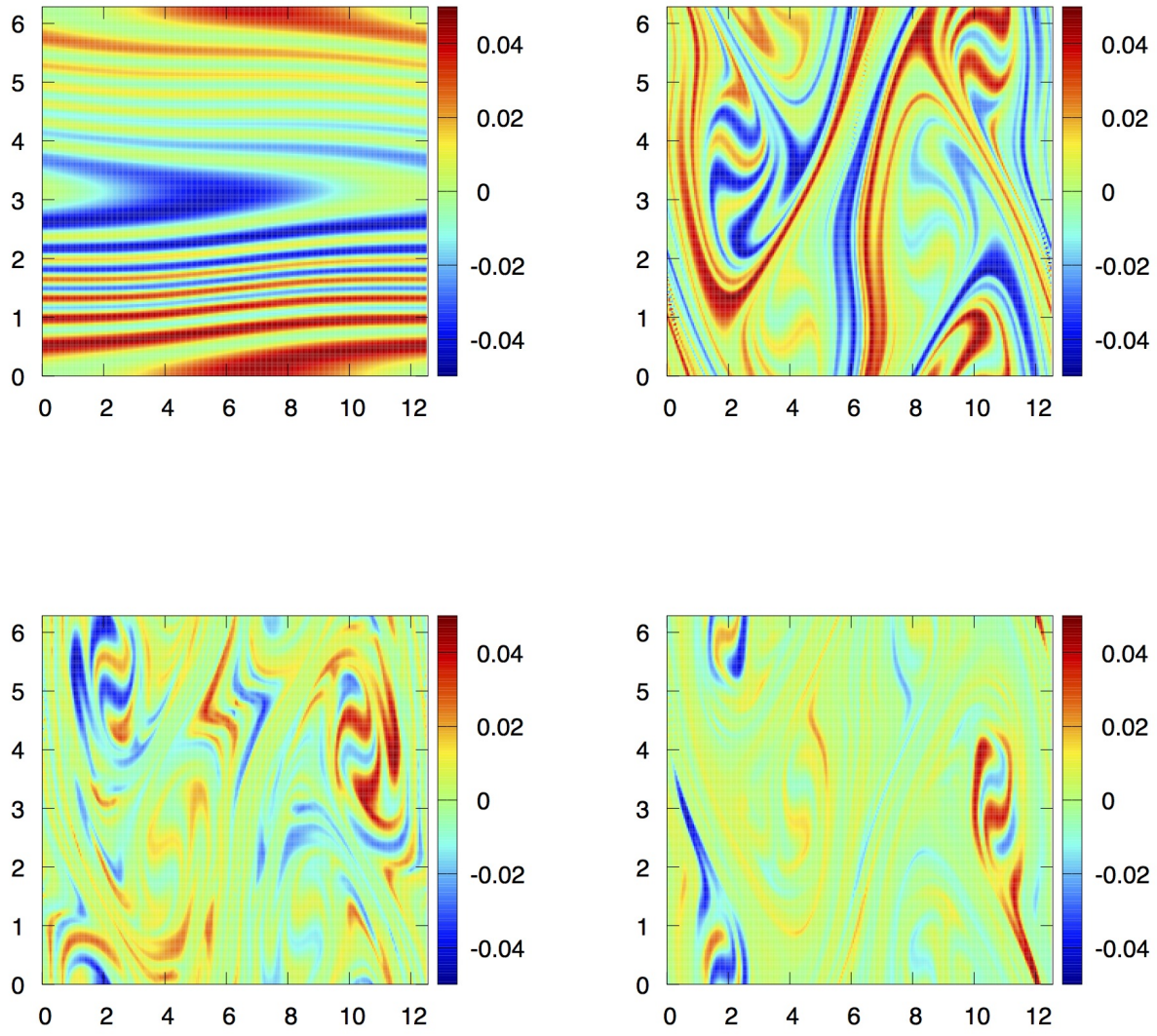

FIGURE 4.8. **Kelvin-Helmholtz instability.** The current density $\mathcal{J}_z$ for the $2d \times 1d$ asymptotic model (4.9). From left to right, top to bottom: $t = 40, 60, 80, 100$.

REFERENCES

[1] T. M. ANTONSEN AND B. LANE, *Kinetic equations for low frequency instabilities in inhomogeneous plasmas*, Phys. Fluids, 23 (1980), pp. 1205–1214.

[2] A. A. ARSEN'EV, *Existence in the large of a weak solution of Vlasov's system of equations*, Ž. Vyčisl. Mat. i Mat. Fiz., 15 (1975), pp. 136–147, 276.

[3] P. BELLAN, *Fundamentals of Plasma Physics*, Cambridge University Press, (2006).

[4] M. BOSTAN, *The Vlasov-Poisson system with strong external magnetic field. Finite Larmor radius regime*, Asymptot. Anal., 61 (2009), pp. 91–123.

[5] F. BOUCHUT, F. GOLSE, AND M. PULVIRENTI, *Kinetic equations and asymptotic theory*, B. Perthame et L. Desvillettes eds, Series in Applied Mathematics, 4 (2000).

[6] J. P. BOYD, *Chebyshev and Fourier spectral methods*, Courier Dover Publications, 2001.

[7] Y. BRENIER, *Convergence of the Vlasov-Poisson system to the incompressible Euler equations*, Comm. in Partial Differential Equations, 25 (2000), pp. 737–754.

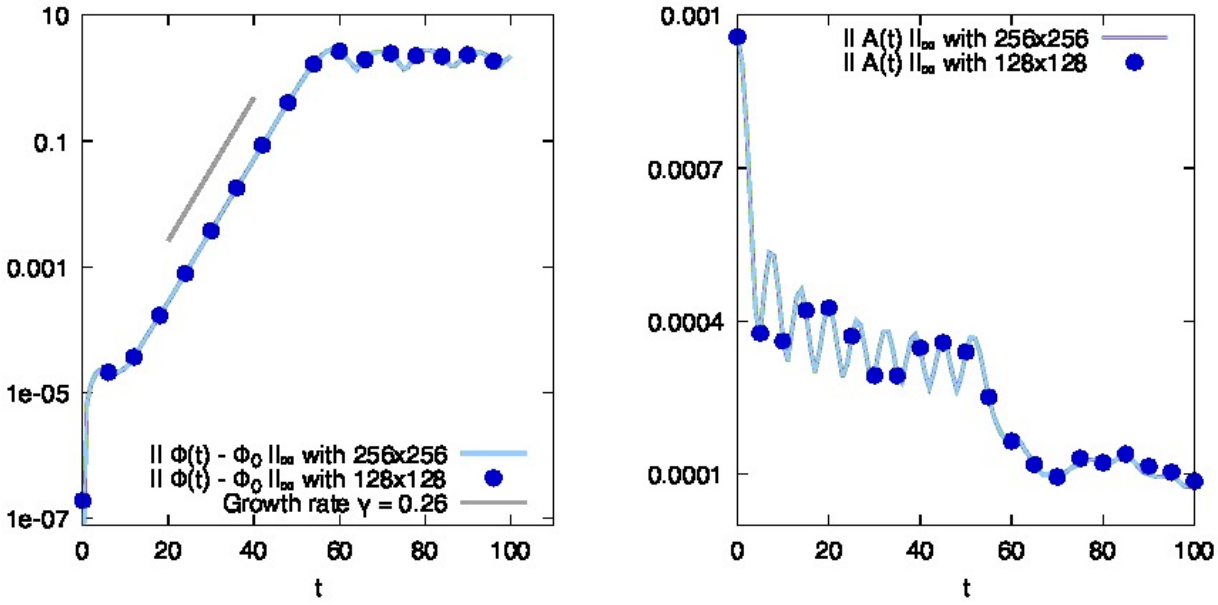

(a) (b)

FIGURE 4.9. **Kelvin-Helmholtz instability.** Time evolution of the norm $\|\Phi(t) - \Phi(0)\|_{L^\infty}$ and $\|A(t) - A(0)\|_{L^\infty}$ for the $2d \times 1d$ asymptotic model (4.9).

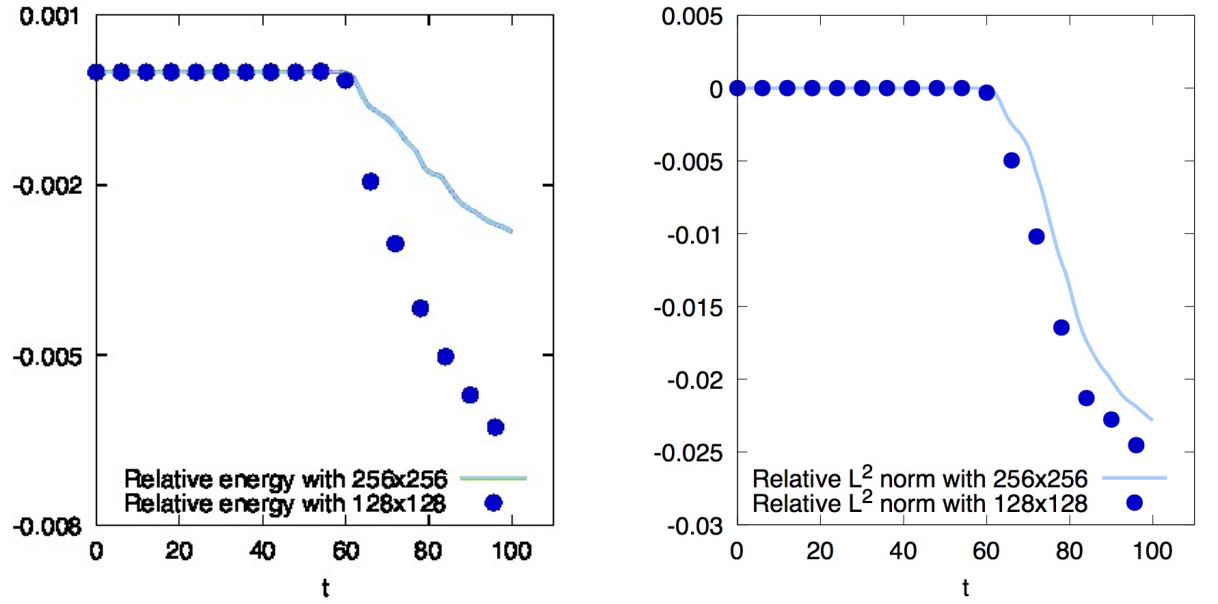

(a) (b)

FIGURE 4.10. **Kelvin-Helmholtz instability.** Time evolution of the relative error of the total energy (2.35), the L^2 norm of F for the $2d \times 1d$ asymptotic model (4.9).

[8] A. J. BRIZARD AND T. S. HAH, *Foundations of Nonlinear Gyrokinetic Theory*, Rev. Modern Phys., 79 (2007), pp. 421–468.
[9] N. CROUSEILLES, M. LEMOU, AND F. MÉHATS, *Asymptotic Preserving schemes for highly oscillatory Vlasov–Poisson equations*, J. Comput. Phys., 248 (2013), pp. 287–308.
[10] N. CROUSEILLES, M. MEHRENBERGER, AND E. SONNENDRÜCKER, *Conservative semi-Lagrangian schemes for Vlasov equations*, J. Comput. Phys., 229 (2010), pp. 1927–1953.
[11] R. C. DAVIDSON, *Physics of nonneutral plasmas*, Imperial College Press London, 2001.

[12] P. Degond and F. Filbet, *On the asymptotic limit of the three dimensional Vlasov-Poisson system for large magnetic field: formal derivation*, arXiv preprint arXiv:1603.03666, (2016).
[13] R. DiPerna and P.-L. Lions, *Solutions globales d'équations du type Vlasov-Poisson*, C. R. Acad. Sci. Paris Sér. I Math., 307 (1988), pp. 655–658.
[14] P.-A. R. E. Frénod and E. Sonnendrücker, *Two-scale expansion of a singularly perturbed convection equation*, J. Math. Pures Appl., 80 (2001), pp. 815–843.
[15] F. Filbet, *Convergence of a finite volume scheme for the Vlasov-Poisson system*, SIAM J. Numer. Anal., 39 (2001), pp. 1146–1169.
[16] F. Filbet and L. M. Rodrigues, *Asymptotically stable particle-in-cell methods for the Vlasov–Poisson system with a strong external magnetic field*, SIAM J. Numer. Anal., 54 (2016), pp. 1120–1146.
[17] F. Filbet and C. Yang, *An inverse Lax–Wendroff method for boundary conditions applied to Boltzmann type models*, J. Comput. Phys., 245 (2013), pp. 43–61.
[18] E. Frénod, S. A. Hirstoaga, M. Lutz, and E. Sonnendrücker, *Long time behaviour of an exponential integrator for a Vlasov-Poisson system with strong magnetic field*, Commun. Comput. Phys., 18 (2015), pp. 263–296.
[19] E. Frénod and E. Sonnendrücker, *Homogenization of the Vlasov equation and of the Vlasov-Poisson system with a strong external magnetic field*, Asymptot. Anal., 18 (1998), pp. 193–213.
[20] E. Frénod and E. Sonnendrücker, *Long time behavior of the two-dimensional Vlasov equation with a strong external magnetic field*, Math. Models Methods Appl. Sci., 10 (2000), pp. 539–553.
[21] F. Golse and L. Saint-Raymond, *The Vlasov-Poisson system with strong magnetic field*, J. Maths. Pures Appl., 78 (1999), pp. 791–817.
[22] ———, *The Vlasov-Poisson system with strong magnetic field in quasineutral regime*, Math. Models Methods Appl. Sci, 13 (2003), pp. 661–714.
[23] D. Han-Kwan, *The three-dimensional finite larmor radius approximation*, Asymptot. Anal., 66 (2010), pp. 9–33.
[24] ———, *Effect of the polarization drift in a strongly magnetized plasma*, ESAIM Math. Model. Numer. Anal., 46 (2012), pp. 929–947.
[25] ———, *On the three-dimensional finite larmor radius approximation: the case of electrons in a fixed background of ions*, Ann. Inst. H. Poincare Anal. Non Linear, 30 (2013), pp. 1127–1157.
[26] M. Hauray and A. Nouri, *Well-posedness of a diffusive gyro-kinetic model*, Ann. Inst. H. Poincare Anal. Non Linear, 28 (2011), pp. 529–550.
[27] R. D. Hazeltine and J. D. Meiss, *Plasma Confinement*, Dover Publications, Mineola, New York, (2003).
[28] R. D. Hazeltine and A. A. Ware, *The drift kinetic equation for toroidal plasmas with large mass velocities*, Plasma Phys., 20 (1978), pp. 673–678.
[29] E. Madaule, S. A. Hirstoaga, M. Mehrenberger, and J. Pétri, *Semi-Lagrangian simulations of the diocotron instability*, Research Report, (2013).
[30] K. Miyamoto, *Plasma Physics and Controlled Nuclear Fusion*, Cambridge University Press, (2006).
[31] M. H. Ph. Ghendrih and A. Nouri, *Derivation of a gyrokinetic model. existence and uniqueness of specific stationary solution*, Kinet. Relat. Models, 2 (2009), pp. 707–725.
[32] L. Saint-Raymond, *Control of large velocities in the two-dimensional gyrokinetic approximation*, J. Math. Pures Appl., 81 (2002), pp. 379–399.
[33] M. M. Shoucri, *A two-level implicit scheme for the numerical solution of the linearized vorticity equation*, International Journal for Numerical Methods in Engineering, 17 (1981), pp. 1525–1538.
[34] E. Sonnendrucker, F. Filbet, A. Friedman, E. Oudet, and J. Vay, *Vlasov simulations of beams with a moving grid*, Computer Physics Communications, 164 (2004), pp. 390–395.
[35] T. Xiong, G. Russo, and J.-M. Qiu, *Conservative multi-dimensional semi-Lagrangian finite difference scheme: Stability and applications to the kinetic and fluid simulations*, arXiv preprint arXiv:1607.07409, (2016).
[36] C. Yang and F. Filbet, *Conservative and non-conservative methods based on Hermite weighted essentially non-oscillatory reconstruction for Vlasov equations*, J. Comput. Phys., 279 (2014), pp. 18–36.

Francis Filbet

Université de Toulouse III & IUF
UMR5219, Institut de Mathématiques de Toulouse,
118, route de Narbonne
F-31062 Toulouse cedex, FRANCE

e-mail: francis.filbet@math.univ-toulouse.fr

Tao Xiong

School of Mathematical Sciences,
Fujian Provincial Key Laboratory of Math. Mod. & HPSC,
Xiamen University, Xiamen, Fujian, P.R. China, 361005.

Université de Toulouse III
UMR5219, Institut de Mathématiques de Toulouse,
118, route de Narbonne
F-31062 Toulouse cedex, FRANCE

e-mail: tao.xiong@math.univ-toulouse.fr

Eric Sonnendrücker

Max Planck Institute for Plasma Physics & Mathematics Center, TU Munich,
Boltzmannstr. 2,
85748 Garching, GERMANY

e-mail: eric.sonnendruecker@ipp.mpg.de